A mathematical model for the energy stored in green roofs

Maria Aguareles[a], Marc Calvo-Schwarzwalder[b,1], Francesc Font[c], Timothy G. Myers[d]

[a] *Department of Computer Science, Applied Mathematics and Statistics, Universitat de Girona, Campus de Montilivi, 17071 Girona, Catalunya, Spain*
[b] *College of Natural and Health Sciences, Zayed University, PO Box 144534 Abu Dhabi, United Arab Emirates*
[c] *Department of Fluid Mechanics, Universitat Politècnica de Catalunya - BarcelonaTech, Av. Eduard Maristany, 16, Edifici A, 08019 Barcelona, Spain*
[d] *Centre de Recerca Matemàtica, Campus de Bellaterra, Edifici C, 08193 Bellaterra, Barcelona, Spain*

Abstract

A simple mathematical model to estimate the energy stored in a green roof is developed. Analytical solutions are derived corresponding to extensive (shallow) and intensive (deep) substrates. Results are presented for the surface temperature and energy stored in both green roofs and concrete during a typical day. Within the restrictions of the model assumptions the analytical solution demonstrates that both energy and surface temperature vary linearly with fractional leaf coverage, albedo and irradiance, while the effect of evaporation rate and convective heat transfer is non-linear. It is shown that a typical green roof is significantly cooler and stores less energy than a concrete one even when the concrete has a high albedo coating. Evaporation of even a few millimetres per day from the soil layer can reduce the stored energy by a factor of more than three when compared to an equivalent thickness concrete roof.

Keywords: Green roof, Heat island, Climate change, Mathematical model
2020 MSC: 93A30, 35K05

1. Introduction

With 55% of the world's population currently living in urban areas the transition from rural living to urbanisation is a global issue. Antrop [1]

[1] Corresponding author: marc.schwarzwalder@zu.ac.ae

predicts that by 2030, 85% of Europe's population will live in urban areas whilst two-thirds of the global population will be in urban areas by 2050 [2]. Increasing levels of urbanisation lead to problems such as poor air and water quality, growing demands on water availability, high energy consumption and a deterioration of the natural environment. Urban areas are also significantly warmer than rural areas, a phenomenon known as the urban heat island effect. Heat islands arise in densely populated regions due to several factors. The albedo of a surface indicates how well it reflects solar energy. Relative to their surroundings, urban areas have high concentrations of dark surfaces such as buildings, roofs, paved surfaces and car parks. These have low albedos and absorb a high percentage of the incoming solar energy. Paved surfaces are typically impermeable, causing rainwater to be directed to drainage systems instead of being absorbed by vegetation which could later cool the area by evapotranspiration. Buildings have high thermal masses, and thus store heat during the day and slowly release it at night whereas natural landscapes such as forest and other green areas consist largely of shaded, air filled regions with a much lower thermal mass, thus storing less heat. Human activities, such as factory and vehicle emissions, heating etc. also impact urban temperatures.

Early heat island studies include Howard's report of the London climate in the late 1800s [3] and Schmidt's meteorological descriptions of urban areas in the early 1900s [4]. Since then heat islands have been observed and examined globally [5, 6]. The resulting higher temperatures are a concern for local authorities and residents. Heat islands can have public health implications such as high temperature ailments, hospitalisation and mortality [7–9]. Circumstances become worse with climate change and heat waves. For example, the 2003 European heat wave resulted in thousands of excess deaths [10]. From an economic perspective, heat islands lead to an increased demand for air conditioning and other cooling equipment, and thus higher electricity costs. Higher temperatures may also lead to a reduction in tourism over the summer months. Thus, there is pressing need for a clear understanding of heat islands, and practical, effective solutions.

To counteract heat islands, local authorities and government bodies are constantly seeking cost-effective, environmentally friendly solutions [11]. One option is a green roof which consists of vegetation planted over a waterproofed system installed on top of a flat or slightly inclined roof. The two main categories of green roofs are extensive and intensive. Extensive green roofs have thin soil with little or no irrigation whereas intensive green roofs have deep soil, an irrigation system and more favourable growing conditions for vegetation. Intensive green roofs typically require a lot of maintenance, whereas extensive green roofs are left to grow naturally with minimal maintenance. Green roofs are made up of various layers including an upper vegetation layer, a growing medium of organic and aggregate materials, a filter membrane to prevent clogging of drains, a drainage layer to inhibit build-up of excess water, a root barrier to stop root penetration and some form of roof support. Green roofs have been shown to reduce the heat island effect as they provide shade, remove heat from the air, and decrease temperatures of roofs and the surrounding air [12–14]. Green roofs have other advantages including rainwater management [15–18], and improvement of air and water quality [19, 20]. They also greatly enhance an urban area's aesthetic value by increasing the level of urban fauna and wildlife habitat.

Modelling heat transfer in green roofs is complicated due to the various layers involved and the movement of moisture [21]. Consequently researchers apply a variety of simplifying hypotheses. Even so the standard approach results in a complex system which must be solved numerically. This is further complicated by the typically 20 different parameter values, many of which are difficult to determine experimentally [22] and therefore require the use of multi-parameter fitting techniques (see [23] for a summary of such models). An attempt to develop a relatively simple model with an analytical solution is contained in the workshop report [24]. In order to produce some preliminary conclusions regarding green roof design this focuses primarily on the energy stored in different substrates subject to constant ambient boundary conditions and a semi-infinite layer. Here we deal primarily with more realistic conditions, where the solar energy and ambient temperature vary during the day, and also a finite thickness substrate. We obtain solutions via separation of variables (verified against numerical solutions) to estimate the energy stored in both extensive and intensive roofs. The ultimate aim being to provide a set of guidelines to aid in the design of green roofs.

Theoretical models dealing with moisture dynamics and heat transport in soil are typically based on those developed by Philip and De Vries in the 1950s [25]. Examples for models extending these descriptions by accounting for energy transport in the soil support and the canopy on top of it include the models presented by Palomo del Barrio [26] or Kondo and Saigusa [27]. Sailor [28] presented a linearized model for determining the temperature evolution at either side of the soil surface, which was later extended by Ouldboukhitine et al. [29]. An extensive review of existing models may be found in Quezada-Garcia et al. [21]. The majority of models incorporate evaporation as a sink term in the soil heat equation, sometimes combined with a term in the boundary condition at the soil surface. Since evaporation is known to be a surface phenomenon, it is more realistic to include it exclusively in the boundary condition.

A number of studies have shown that plants have some ability to regulate their temperature over a wide range of ambient temperatures, see [30–32].

Citing these studies, and many others, Michaletz et al. [33] point out that the difference between the plant and air temperature is generally small and the correspondence is particularly close for ambient temperatures in the range 20-30°C. The correspondence is achieved primarily through evapotranspiration. Air has a very low viscosity (approximately 1.8×10^{-5} Pa s) and so is easily mixed, for example by the motion of air above the canopy, motion of the plants or convective currents due to temperature differences between the air and the soil. Palomo [26] discusses the turbulent nature of the air both in and above the canopy (and states that as a consequence of this the energy and mass fluxes cannot be exactly predicted). It is well known from fluid mechanics studies that turbulent diffusion is orders of magnitude greater than thermal diffusion: as soon as turbulent diffusion occurs the air temperature may be assumed approximately constant (and so set to the ambient value).

Given this dynamic mechanism for maintaining the air and plant temperature at a similar level as well as the tendency for turbulent mixing of the air, when developing a mathematical model the thermal response of the canopy may be partially decoupled from that of the soil. Specifically the canopy affects the soil in that the canopy air removes or adds heat by convection while the leaves provide shade. However, any energy that the soil gives to the air is rapidly transported away through turbulent diffusion and has a negligible effect on the surroundings. Plants also remove water from the soil, which affects the thermophysical parameter values. Consequently, if the layers are to be decoupled it must be under the assumption that water removal is relatively small, which may come through investigating situations with a low evapotranspiration rate or for short times.

As a consequence of the above arguments, in this paper we will focus on the development of a simple mathematical model to determine the effect of different substrates on energy stored during daylight hours (which here we will define as when the solar irradiance is above zero). This energy can then go to heating the surface or be released at night, both with detrimental effects on the comfort and energy footprint in the local area. The model requires a number of assumptions. With regard to evaporation we assume that the mass loss is proportional to the (varying) surface temperature. We also assume an approximately constant moisture content in the soil. This requires studying situations involving the removal of a few millimetres of water per day, which is not a strong restriction, and only carry out calculations for a single day. Subsequent days may be dealt with by imposing new initial conditions. The resulting mathematical model is simple enough to be solved analytically and the thermal performance of the layer can be ultimately described by a single expression. The ultimate goal being to provide a set of guidelines to demonstrate the effect of substrate type and physical characteristics (depth, composition etc) on the energy storage and to provide simple explicit formulae to compute this energy.

The paper is organised as follows. In Section 2 we specify the model assumptions to obtain the governing heat equation in the roof layer as well as the surface boundary condition which accounts for heat transfer due to convection, radiation, solar irradiance and surface evaporation. In Section 3 exact and approximate analytical solutions are obtained for both intensive and extensive green roofs. In Section 4 we analyse different roof configurations and discuss the range of validity of the different approximations obtained in the previous section. Finally, Section 5 is devoted to the conclusions.

2. Derivation of governing equations

The mathematical model will be developed subject to the following assumptions:

1. The plant temperature is close to the air temperature [33].
2. The air forms an infinite sink and is well mixed, so the air temperature may be assumed independent of the plant cover and substrate.
3. The plants have two main effects on the soil, firstly they provide shade (so reducing the amount of solar energy available to be absorbed), secondly they remove water through transpiration.
4. The variation in the soil moisture is small such that it does not produce any significant variation in the thermal parameters.
5. The temperature flow is predominantly one-dimensional.

The first four assumptions were discussed in the introduction. The assumption on the moisture content obviously imposes restrictions on the calculation time, which must be sufficiently small that only small quantities of water evaporate, or that the substrate is carefully watered at regular intervals. This is perhaps the most restrictive assumption, as well as the conditions it imposes on the time the moisture content affects the albedo and the thermal properties (such as density and thermal conductivity). Our results may therefore be viewed as providing bounds on the energy storage capacity for different moisture levels.

Regarding the final assumption, our aim is to produce a simple model capable of predicting and providing insight into a green roof's performance. Given that the main drivers for energy change occur at the top and bottom boundaries it seems apparent that the heat flow is predominantly perpendicular to the surface. Small local changes, for example due to variations in leaf coverage, would require a detailed analysis for each individual green roof. By dealing with the one-dimensional problem we are effectively considering the average temperature over a cross-sectional area.

Table 1: Summary of the symbols used in this work.

Symbols

A	Albedo (-)
H_{as}	Air-soil heat transfer coefficient (W/m^2°C)
ρ	Density (kg/m^3)
f, g	Deviation from average irradiance, temperature (W/m^2, °C)
z	Distance from surface (m)
E	Energy absorbed (J/m^2)
λ_n	Eigenvalue (-)
φ_n, ϕ_n, ψ_n	Eigenfunction (-)
d, $\dot{d}$	Evaporated amount, Evaporation rate (m, m/s)
α	Evaporation proportionality constant (m/°Cs)
F_{VC}	Fractional vegetative coverage (-)
q	Heat flux (W/m^2)
ϵ	Heat loss parameter (-)
L_e	Latent heat of evaporation (J/kg)
p	period (s)
L	Soil thickness (m)
C_1, C_2	Specific energy terms (W/m^2, W/m^2°C)
c	Specific heat capacity (J/kg°C)
Q	Sun irradiance (W/m^2)
T	Temperature (°C)
k	Thermal conductivity (W/m°C)
D	Thermal diffusivity (m^2/s)
t	Time (s)

Superscripts

0	Constant environmental conditions

Subscripts

s	Soil	c	Concrete	a	Air
w	Water	rad	Radiation	conv	Convection
evap	Evaporation	lap	Laplace	tot	Total
max	Maximum value	min	Minimum value	mn	Mean value
av	Average value	num	Numerical	app	Approximate
net	Net value				

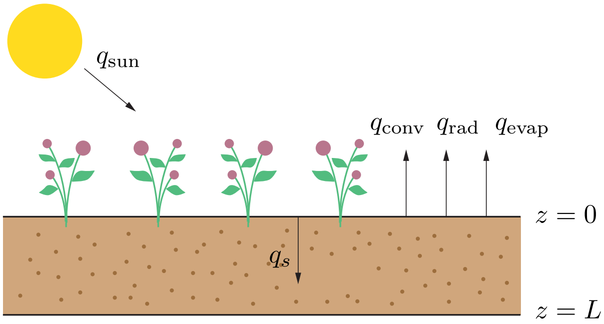

Figure 1: Illustration of the green roof model.

2.1. Mathematical model

The one dimensional model that we will consider is represented in Figure 1. Subject to the above restrictions the substrate satisfies the one-dimensional heat equation

$$\rho_s c_s \frac{\partial T}{\partial t} = \frac{\partial}{\partial z}\left(k_s \frac{\partial T}{\partial z}\right) , \tag{1}$$

where the notation is described in Table 1. The thermal parameters may depend on the water content (here assumed to be constant) and the substrate occupies the region $z \in [0, L]$, with $z = 0$ being open to the atmosphere. With constant coefficients we denote the thermal diffusivity as $D_s = k_s/\rho_s c_s$. At the surface, $z = 0$, the energy conducted into or out of the substrate must balance the incoming heat from the sun with that lost through convection, radiation and evaporation, hence

$$q_s = -k_s \left.\frac{\partial T}{\partial z}\right|_{z=0} = q_{\text{sun}} + q_{\text{conv}} + q_{\text{rad}} + q_{\text{evap}} \, . \tag{2}$$

As for the lower boundary conditions, we assume the roof has a perfect thermal insulation, so there is no heat flowing out of the roof and into the house, which can be written in terms of a homogeneous Neumann boundary condition like $\partial T(L, t)/\partial z = 0$. However, if the soil is deep enough the domain can be assumed to be semi-infinite where the temperature far from the surface remains constant, which can be written like $\partial T(z, t)/\partial z \to 0$ as $z \to \infty$. We shall therefore consider one of the two following boundary conditions:

$$\text{i)} \ \lim_{z\to\infty} \frac{\partial T}{\partial z} = 0 \, , \qquad \text{ii)} \ \left.\frac{\partial T}{\partial z}\right|_{z=L} = 0 \, . \tag{3}$$

The first applies to thick soil layers, the second to thinner layers. Clearly, due to weight considerations, green roofs are far from semi-infinite: later we will discuss what constitutes thick and thin and demonstrate that, at least mathematically, roofs greater than 15cm thick may be treated as semi-infinite.

As initial condition we shall take the daily mean temperature value,

$$T(z,0) = T_{\mathrm{mn}} = \frac{T_{\max} + T_{\min}}{2} \,. \tag{4}$$

2.2. Specific energy terms

The most important part of the above energy balance is the surface boundary condition, equation (2) which requires expressions for the convection, radiation and evaporation terms.

Convection and radiation. Firstly we note that the convective and radiation terms are usually combined to make a single effective heat transfer term. The sum of the convective and radiation terms is

$$E_{conv} + E_{rad} = -H'_{as}(T - T_a) - \epsilon\sigma(T^4 - T_a^4)\,, \tag{5}$$

where H'_{as} is the soil-air heat transfer coefficient, T_a is the ambient air temperature, ϵ is an emissivity coefficient and σ is the Stefan–Boltzmann constant. Assuming the soil surface temperature is not greatly different to the air temperature we may write $T = T_a + f$, where $f = (T - T_a) \ll T_a$, then

$$(T^4 - T_a^4) = (T_a^4 + 4fT_a^3 + 6f^2T_a^2 \cdots) - T_a^4 = 4fT_a^3\left(1 + \frac{3}{2}\frac{f}{T_a} + \cdots\right) \,. \tag{6}$$

Provided $f/T_a = (T - T_a)/T_a \ll 1$, then

$$E_{conv} + E_{rad} \approx -H_{as}(T - T_a) \tag{7}$$

where $H_{as} = H'_{as} + 4\epsilon\sigma T_a^3$ is a combined soil-air heat transfer coefficient.

Energy flux related to the sun irradiance. The solar energy term in (2) may be written as

$$q_{\mathrm{sun}} = (1 - F_{VC})(1 - A_s)Q_{\mathrm{net}}\,, \tag{8}$$

where A_s is the substrate albedo and Q_{net} the net irradiance received from the sun. The parameter $F_{VC} \in [0,1]$ is the fractional vegetative coverage, a dimensionless quantity for whose definition we may use the Leaf Area Index (LAI), see [21, 26, 34], which is used to characterise plant canopies. The LAI is defined as the one-sided green leaf area per unit ground surface area (see for instance [35]). Since dense plant canopies can have several layers of leafs, values of LAI > 1 are permissible. Plant leaves very rapidly prevent the sun from reaching the soil surface, so a common definition has $F_{VC} = 1 - \exp(-\mathrm{LAI})$.

Energy loss due to evaporation. Evaporation is a form of phase change which occurs below the standard phase change temperature. For fluid molecules to escape from the liquid surface they require sufficient energy. At low temperatures the fluid molecules have low energy, however they may gain above average energy through collisions with other molecules. The closer to the phase change temperature the more likely it is that a molecule will gain sufficient energy to break free from the liquid and join the vapour layer above the surface. For this reason we will define an evaporation rate proportional to the surface temperature $\dot{d} = \alpha T(0,t)$, that is, the evaporation rate increases with the surface temperature and so

$$q_{\text{evap}} = -\rho_w L_e \dot{d}(t) = -\rho_w L_e \alpha T(0,t)\,, \tag{9}$$

where $\dot{d}$ the rate at which water is evaporated per unit area. The constant of proportionality α in fact depends on quantities such as the relative humidity, air flow, surface roughness which all influence the evaporation but will here be taken as a constant.

The soil surface boundary condition may now be written as

$$\begin{aligned} -k_s \frac{\partial T}{\partial z}\bigg|_{z=0} =& (1 - F_{VC})(1 - A_s) Q_{\text{net}} \\ & - H_{as}(T(0,t) - T_a) - \rho_w L_e \alpha T(0,t)\,. \end{aligned} \tag{10}$$

The relation between the boundary condition (10) and the Penman-Monteith (PM) equation is discussed in [24]. The PM equation is a widely used formula primarily aimed at estimating the amount of evapotranspiration. It includes a variety of empirical quantities, some, such as the 'ground heat flux', are difficult to measure. The ground heat flux is identical to $-k_s T_z(0,t)$ which here will be determined during the solution process. As discussed earlier transpiration plays a limited role in the substrate energy balance. The surface boundary condition depends on the surface evaporation whereas transpiration acts to remove water from within the soil which is then evaporated in the plant layer and the associated energy passed to the air. The effect of transpiration on the soil is then purely through the amount of water removed. Experimentally this may lead to an issue in distinguishing where the water has been removed, since this affects the measurement of d. In which case we could make an estimate via an empirical formula. However, our goal here is to provide a comparative study of different forms and depths of roof so we will simply specify a value for d and then see how it affects the different substrates.

Time-dependent environment conditions. Both the solar energy and ambient temperature vary throughout the day, typical forms are shown in Figure 2.

The solid curve in Figure 2(a) depicts the variation of solar radiation. We take the origin of our time axis as the moment when the solar radiation first reaches the surface and, in this example, the radiation returns to zero at the end time $t_f = 14$ hours (note, the calculations are in SI units so in all equations we work in seconds, $t_f = 14 \times 3600$s). Consequently we approximate the irradiance by

$$Q_{\rm net}(t) = Q_{\rm max} \sin\left(\frac{2\pi t}{p_1}\right) , \tag{11}$$

where the period is $p_1 = 2t_f$ s. This holds for $t \in [0, t_f]$ s, which is how we define our daytime and is the time period over which we will calculate the energy absorbed by the substrate. In Figure 2(b) the solid curve represents the ambient temperature. This reaches a minimum a short time after the solar radiation begins, while the maximum occurs shortly after the peak of radiation. If we choose a minimum at $t = t_{\rm min} = 1$ hour and a maximum at $t = t_{\rm max} = 9$ hours then the sine wave representation takes the form

$$T_a(t) = T_{\rm mn} - \frac{\Delta T}{2} \cos\left(\frac{2\pi\,(t - t_{\rm min})}{p_2}\right) , \tag{12}$$

where $\Delta T = T_{\rm max} - T_{\rm min}$ and the period p_2 is twice the distance between the maximum and minimum, $p_2 = 2\,(t_{\rm max} - t_{\rm min}) = 2 \times 8 \times 3600$s. Given that neither period p_1 or p_2 coincide with the day length these functions cannot be applied for a full 24 hours. However, our goal is to calculate the energy absorbed by the substrate over daylight hours in which case the definitions (11, 12) provide a realistic approximation.

In the following sections we will calculate analytical and numerical solutions for the temperature and energy in the substrate. Some of the analytical approximations employed will require constant values for irradiance and ambient temperature and thus some form of average value must be determined. Consequently we write

$$Q_{\rm net}(t) = Q_{\rm av} + f(t) \, , \qquad T_a(t) = T_{\rm av} + g(t) \, . \tag{13}$$

To determine the average solar irradiance we first calculate the daily total (i.e., the solar exposure or insolation)

$$Q_{\rm tot} = Q_{\rm max} \int_0^{t_f} \sin\left(\frac{2\pi t}{p_1}\right) \, {\rm d}t = \frac{2}{\pi} Q_{\rm max} t_f \, , \tag{14}$$

where we have used $p_1 = 2t_f$. Similarly, the integral of the temperature

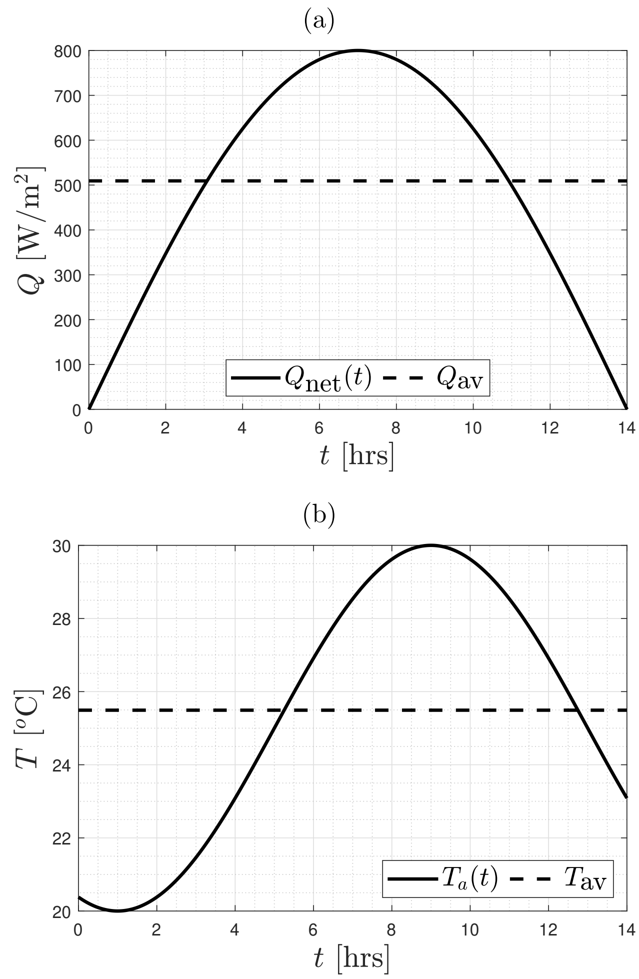

Figure 2: (a) Evolution of the solar energy (irradiance) and (b) the air temperature during solar radiation hours. The dashed lines represent the daily averages.

during the time period $[0, t_f]$ is

$$\begin{aligned} T_{\rm tot} &= \int_0^{t_f} T_a(t)\,\mathrm{d}t \\ &= T_{\rm mn} t_f - \frac{\Delta T p_2}{4\pi}\left[\sin\left(\frac{2\pi\,(t_f - t_{\rm min})}{p_2}\right) + \sin\left(\frac{2\pi t_{\rm min}}{p_2}\right)\right] . \quad (15) \end{aligned}$$

The daily averages are then

$$Q_{\rm av} = \frac{Q_{\rm tot}}{t_f}\,, \qquad T_{\rm av} = \frac{T_{\rm tot}}{t_f}\,. \quad (16)$$

The daily average temperature, $T_{\rm av}$, and the mean temperature, $T_{\rm mn}$, are only equal if $t_f = p_2$, this would occur with exactly 12 hours of daylight.

Substituting for $T_{\text{av}}, Q_{\text{av}}$ in equations (13) defines $f(t), g(t)$

$$f(t) = Q_{\max}\left(\sin\left(\frac{2\pi t}{p_1}\right) - \frac{2}{\pi}\right), \tag{17}$$

$$\begin{aligned} g(t) =& \frac{\Delta T}{2}\left(\frac{p_2}{2\pi t_f}\left[\sin\left(\frac{2\pi(t_f - t_{\min})}{p_2}\right) + \sin\left(\frac{2\pi t_{\min}}{p_2}\right)\right]\right. \\ & \left. - \cos\left(\frac{2\pi(t - t_{\min})}{p_2}\right)\right). \end{aligned} \tag{18}$$

The final form for the surface boundary condition is then

$$-k_s \left.\frac{\partial T}{\partial z}\right|_{z=0} = C_1 + G(t) - C_2 T(0,t), \tag{19}$$

where C_1, C_2 are constant and $G(t)$ incorporates the $f(t), g(t)$ terms:

$$C_1 = (1 - F_{VC})(1 - A_s)Q_{\text{av}} + H_{as}T_{\text{av}}, \qquad C_2 = H_{as} + \rho_w L_e \alpha, \tag{20}$$

$$G(t) = (1 - F_{VC})(1 - A_s)f(t) + H_{as}g(t). \tag{21}$$

Energy flux due to evaporation. With regard to the evaporation rate we first note that the value of the constant α must be consistent with the specified daily evaporation rate. If we observe that d metres have evaporated in time t_f then

$$d = \int_0^{t_f} \dot{d}\,\mathrm{d}t = \alpha \int_0^{t_f} T(0,t)\,\mathrm{d}t. \tag{22}$$

In the case where $\dot{d}$ is constant the above equation states that $\dot{d} = d/t_f$ and α is redundant. In the variable case the method to obtain α from this relation will be discussed later.

2.3. Absorbed energy

To determine the energy absorbed (above the initial energy) in a layer of thickness L we must evaluate

$$E(t) = \int_0^L \rho_s c_s (T(z,t) - T_{\text{mn}})\,\mathrm{d}z. \tag{23}$$

We note that the energy is related to the surface boundary condition and, in turn, to the evaporation rate. Indeed, integrating (1) with respect to time and using (19) one obtains

$$\frac{dE}{dt} = k_s \left.\frac{\partial T}{\partial z}\right|_{z=L} - k_s \left.\frac{\partial T}{\partial z}\right|_{z=0}. \tag{24}$$

With an insulated layer $\partial T/\partial z = 0$ at $z = L$, whereas for a deep layer $T \to T_\infty$ as $z \to \infty$, hence $\partial T/\partial z \to 0$. In either case the first temperature derivative in (24) may be neglected while the second is simply the energy flux at the surface which is defined by the surface boundary condition

$$\frac{dE}{dt} = C_1 + G(t) - C_2 T(0,t)\,, \tag{25}$$

and therefore the energy absorbed in the layer is

$$E(t) = C_1 t + \int_0^t (G(\tau) - C_2 T(0,\tau))\ \mathrm{d}t\,. \tag{26}$$

According to the definition of $G(t)$ given in (21), $\int_0^{t_f} G(t)\mathrm{d}t = 0$. Therefore, the energy absorbed at the end of the day, and thus available for release through the night, is

$$\begin{aligned} E(t_f) &= C_1\,t_f - C_2 \int_0^{t_f} T(0,t)\,\mathrm{d}t = C_1 t_f - C_2 \frac{d}{\alpha} && (27)\\ &= (1 - F_{VC})(1 - A_s) Q_{\mathrm{av}} t_f - \rho_w L_e d + H_{as}\left(T_{\mathrm{av}} t_f - \frac{d}{\alpha}\right)\,. && (28)\end{aligned}$$

It would appear that we can finish the calculation here given that we have an expression for the energy absorbed through the day and hence the energy available for release at night. The simplicity of the above expression clearly shows how the absorbed energy depends on the problem parameters. However, α is *a priori* unknown and depends on the surface temperature. Consequently in the following sections we will investigate the temperature flow more carefully to determine the evaporation rate and specifically the form of the function $d(\alpha)$. Further, this will determine the surface temperature which is an important quantity in the comfort of the population. Importantly the analysis will show that due to the interplay between evaporation and surface temperature the absorbed energy does not depend linearly on t_f as suggested by the above result.

2.4. Numerical solution

The mathematical problem defined by the heat equation (1), boundary conditions (3i) and 10 and the initial condition (4) can be solved numerically by using Matlab's built-in function `pdepe`, which performs a discretization of the spatial variable to obtain a system of ODEs which is then solved using the function `ode15s`. It is an excellent way to demonstrate the accuracy of the analytical solutions but does not provide any insight into the role of the model parameters.

3. Analytical solutions

In this section we seek analytical solutions for both infinite and finite depth layers. Specifically we will calculate the temperature profile throughout the layer and from this determine the surface temperature which is required to calculate the energy absorbed throughout the day. We note that in the case of a substrate with infinite depth the analytical method requires constant average values for the ambient temperature and solar irradiance (as studied in [24]).

3.1. Deep substrate solution for averaged input values

As discussed above, for thick layers the surface temperature variation may not affect the lower boundary $z = L$. Consequently we may seek an analytical solution based on the assumption $L \to \infty$ (and subsequently determine a lower bound for this approximation).

Taking the average values for the ambient temperature and solar radiation discussed in Section 2.2, that is $G = 0$, we may use Laplace transforms (see Appendix A) to obtain

$$\begin{aligned} T_{\mathrm{lap}}(z,t) =& T_{\mathrm{mn}} + \frac{C_1 - C_2 T_{\mathrm{mn}}}{C_2}\Bigg[\mathrm{erfc}\left(\frac{z}{2\sqrt{D_s t}}\right) \\ & - \exp\left(\frac{C_2}{k_s}\left(\frac{C_2 D_s t}{k_s} + z\right)\right)\mathrm{erfc}\left(\frac{z}{2\sqrt{D_s t}} + \frac{C_2\sqrt{D_s t}}{k_s}\right)\Bigg], \end{aligned} \tag{29}$$

where $\mathrm{erfc}(z)$ is the well known complementary error function,

$$\mathrm{erfc}(z) = \frac{2}{\sqrt{\pi}}\int_z^\infty e^{-t^2}\,\mathrm{d}t\,.$$

In the limit $z \to \infty$ this gives $T \to T_{\mathrm{mn}}$ which satisfies $\partial T/\partial z \to 0$ so this applies for both boundary conditions (3) for sufficiently large values of L. The surface temperature is simply

$$T_{\mathrm{lap}}(0,t) = T_{\mathrm{mn}} + \frac{C_1 - C_2 T_{\mathrm{mn}}}{C_2}\left[1 - \exp\left(\frac{C_2^2 D_s}{k_s^2}t\right)\mathrm{erfc}\left(\frac{C_2\sqrt{D_s t}}{k_s}\right)\right]. \tag{30}$$

Using expression (23) the energy absorbed throughout the layer after time t is

$$\begin{aligned} E_{\mathrm{lap}}(t) =& \frac{k_s^2}{D_s C_2^2}(C_1 - C_2 T_{\mathrm{mn}})\Bigg[\exp\left(\frac{C_2^2 D_s}{k_s^2}t\right) \\ & \times \mathrm{erfc}\left(\frac{C_2}{k_s}\sqrt{D_s t}\right) + \frac{2}{\sqrt{\pi}}\frac{C_2}{k_s}\sqrt{D_s t} - 1\Bigg]. \end{aligned} \tag{31}$$

We note that $E_{\text{lap}}(t)$ is linear in C_1 (defined in (20)), this is in keeping with equation (27) although the time dependence is different. The dependence of the energy on the evaporation rate, which appears in C_2, is not so clear. We can find a simpler expression by considering large time solutions, i.e. approaching the end of the day. For the soils considered in this work $C_2\sqrt{D_s t_f/k_s}$ takes values between 2 and 5. Noting that for large y, $e^{y^2}\text{erfc}(y) = 1/(y\sqrt{\pi}) + \mathcal{O}(1/y^3)$. For sufficiently large times the energy may then be approximated by

$$E_{\text{lap}}(t) \sim \frac{k_s^2}{D_s C_2^2}(C_1 - C_2 T_{\text{mn}})\left[\frac{k_s}{C_2\sqrt{D_s t}} + \frac{2}{\sqrt{\pi}}\frac{C_2}{k_s}\sqrt{D_s t} - 1\right]. \tag{32}$$

For t close to t_f the second term in the square brackets is dominant indicating

$$\begin{aligned} E_{\text{lap}}(t_f) \to& 2\left(\frac{C_1}{C_2} - T_{\text{mn}}\right)\frac{k_s}{\sqrt{\pi D_s}}\sqrt{t_f} && (33)\\ =& 2\Bigg(\frac{(1-F_{VC})(1-A_s)Q_{\text{av}} + H_{as}T_{\text{av}}}{H_{as} + \rho_w L_e \alpha} \\ & - \frac{T_{max} + T_{min}}{2}\Bigg)\sqrt{\frac{\rho_s c_s k_s t_f}{\pi}}\,. && (34) \end{aligned}$$

This simple expression provides an estimate of the energy for a deep substrate layer when the average of irradiance and ambient temperature are imposed. It clearly indicates the effect of each system parameter. There is a linear dependence on the fractional vegetative coverage, albedo and irradiance. The theromophysical parameters, ρ_s, c_s, k_s appear as a square root.

3.2. Finite substrate solution

Here we consider a finite substrate on top of an insulating layer. In this case we apply the boundary condition (3 ii). The heat equation (1) is now defined over the finite domain $z \in [0, L]$, which suggests a solution by separation of variables. This leads to an approximate solution of the form

$$T(z,t) = T_{\text{mn}} + \frac{C_1 L}{k_s}\sum_{n=1}^{\infty}\frac{\cos(\lambda_n)}{\lambda_n^2 + \beta_3\cos^2(\lambda_n)}\cos\left(\lambda_n\left(1 - \frac{z}{L}\right)\right)\psi_n(t)\,. \tag{35}$$

The derivation is provided in Appendix B. The eigenvalues satisfy

$$\tan(\lambda_n) = \frac{\beta_3}{\lambda_n}\,. \tag{36}$$

and

$$\psi_n(t) = \beta_2\left[1 - \exp\left(-\frac{\lambda_n^2 D_s t}{L^2}\right)\right] + \lambda_n^2 \mathcal{G}_n(t)\,, \tag{37}$$

where $\mathcal{G}_n(t) = \beta_1 I_{1,n}(t) + (1-\beta_1) I_{2,n}(t)$ and

$$\begin{aligned} I_{1,n}(t) =& \frac{D_s L^2 p_1 \pi}{8\pi^2 L^4 + 2 D_s^2 p_1^2 \lambda_n^4} \left[\frac{D_s p_1 \lambda_n^2}{L^2} \sin\left(\frac{2\pi t}{p_1}\right) - 2\pi \cos\left(\frac{2\pi t}{p_1}\right) \right. \\ & \left. + 2\pi \exp\left(-\frac{\lambda_n^2 D_s t}{L^2}\right) \right] - \frac{1}{\lambda_n^2} \left[1 - \exp\left(-\frac{\lambda_n^2 D_s t}{L^2}\right) \right], \end{aligned} \tag{38}$$

$$\begin{aligned} I_{2,n}(t) =& \frac{1}{\lambda_n^2} \left(\frac{T_{\mathrm{mn}}}{T_{av}} - 1\right) \left[1 - \exp\left(-\frac{\lambda_n^2 D_s t}{L^2}\right) \right] \\ & + \frac{\Delta T D_s^2 p_2^2 \lambda_n^2}{2 T_{av} \left(4\pi^2 L^4 + D_s^2 p_2^2 \lambda_n^4\right)} \left[\exp\left(-\frac{\lambda_n^2 D_s t}{L^2}\right) \cos\left(\frac{2\pi t_{\min}}{p_2}\right) \right. \\ & \left. - \cos\left(\frac{2\pi \left(t - t_{\min}\right)}{p_2}\right) \right] - \frac{\Delta T D_s L^2 p_2 \pi}{T_{av} \left(4\pi^2 L^4 + D_s^2 p_2^2 \lambda_n^4\right)} \\ & \times \left[\exp\left(-\frac{\lambda_n^2 D_s t}{L^2}\right) \sin\left(\frac{2\pi t_{\min}}{p_2}\right) + \sin\left(\frac{2\pi \left(t - t_{\min}\right)}{p_2}\right) \right], \end{aligned} \tag{39}$$

where $p_1 = 2 t_f$ and $p_2 = 2\left(t_{\max} - t_{\min}\right)$. These expressions involve three non-dimensional parameters

$$\beta_1 = \frac{(1 - F_{VC})(1 - A_s) Q_{\mathrm{av}}}{C_1}, \quad \beta_2 = 1 - \frac{C_2 T_{\mathrm{mn}}}{C_1}, \quad \beta_3 = \frac{C_2 L}{k_s}. \tag{40}$$

Setting $z = 0$ in (36) gives the surface temperature

$$T_{\mathrm{N}}(0,t) = T_{\mathrm{mn}} + \frac{C_1 L}{k} \sum_{n=1}^{\infty} \frac{\psi_n(t)}{\lambda_n^2 + \beta_3^2 + \beta_3}. \tag{41}$$

The eigenvalues, λ_n, are found through the numerical solution of (36). In the following we will also employ an approximation to the first eigenvalue

$$\lambda_1 \approx \lambda_{\mathrm{app}} = \left(\frac{5^{1/3}}{6} y - \frac{5}{6} - \frac{13 \cdot 5^{2/3}}{6y} \right)^{1/2} \tag{42}$$

where

$$y = \left(110 + 162\beta_3 + 9\sqrt{285 + 440\beta_3 + 324\beta_3^2} \right)^{1/3}, \tag{43}$$

see Appendix B.

In Figure 3 we compare the exact and approximate values of λ_1 for varying L and parameter values for a typical soil (parameter values used here and in the next three figures are discussed in detail in §4). As may be seen, the error

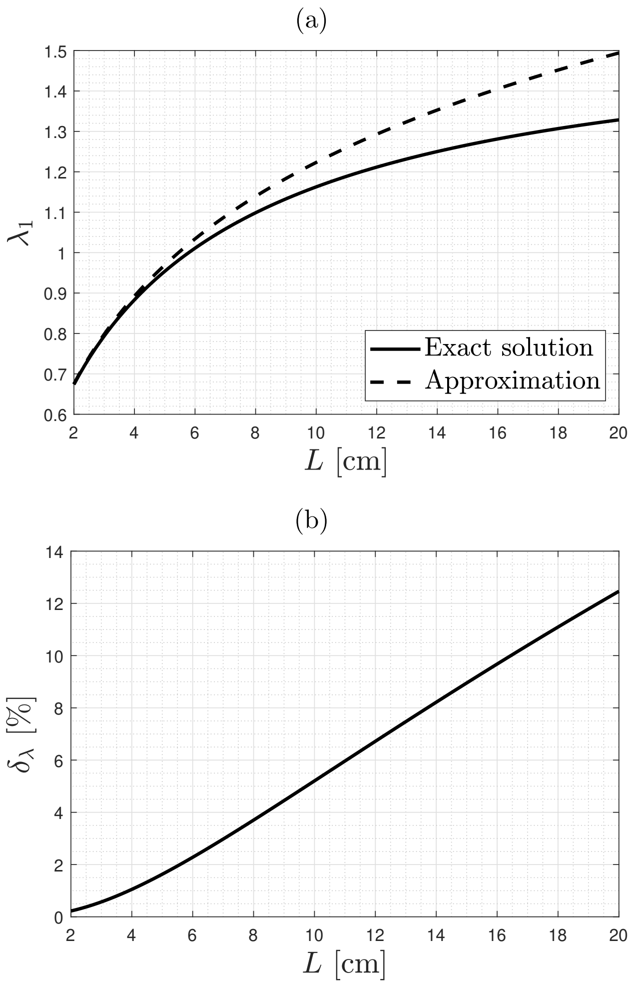

Figure 3: (a) Value of λ_1 according to the numerical solution of (36) and the approximation (42). (b) Relative error of the approximation (42), defined by $\delta_\lambda = 100 \times |\lambda_{1,\text{num}} - \lambda_{1,\text{approx}}| / \lambda_{1,\text{num}}$.

grows with L. When $L = 16$cm the error is around 10%, beyond this depth we should expect solutions using this approximation to exhibit significant errors.

In practice, we can only use a finite amount of terms, hence we call T_N the approximation that uses N terms of the series (35). The energy (to N terms) absorbed within the layer is found by integrating (35)

$$E_{\text{N}}(t) = \frac{L^2 C_1}{D_s} \sum_{n=1}^{N} \frac{\beta_3 \psi_n(t)}{\lambda_n^4 + \lambda_n^2 \beta_3 (1 + \beta_3)} \,. \tag{44}$$

Again we may observe a strong dependence on C_1, which represents the energy gains. However, both C_1 and the energy loss term C_2 appear in ψ_n while $\beta_3 = C_2 L/k_s$, so the dependence is not so clear as for the thick substrate.

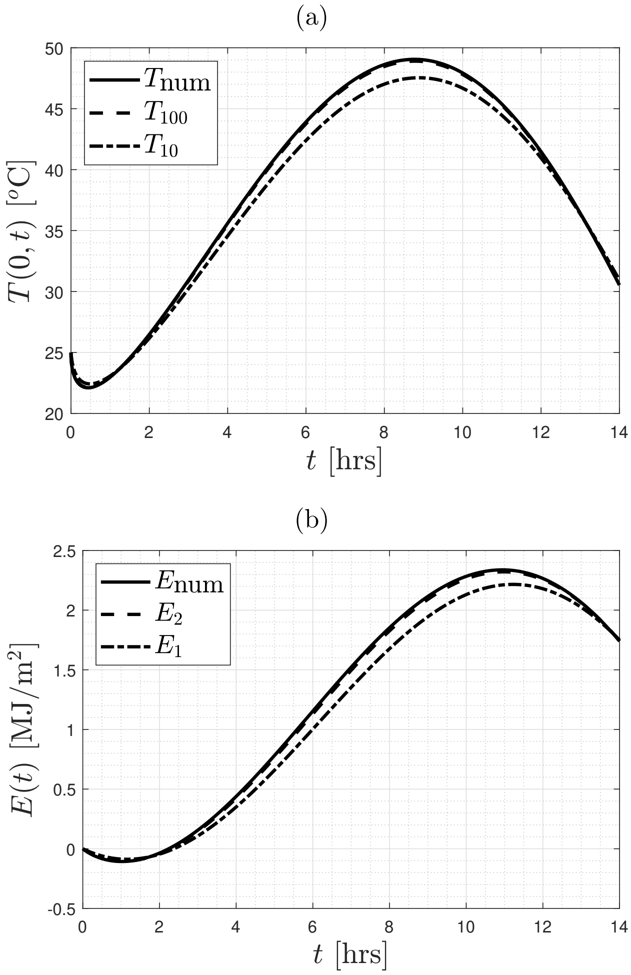

Figure 4: (a) Evolution of the surface temperature using the numerical solution and equation (41) retaining 10 and 100 terms in the expansion. (b) Evolution of the stored energy using the numerical solution and expression (44) with $N = 1, 2$.

In Figure 4 the series solution is compared with a numerical solution obtained using the Matlab *pdepe* function (parameter values are given in §4, the value $\alpha = 10^{-9}$m/°Cs). In the case of the surface temperature the convergence rate of the series is slow such that only as $N \to 100$ do the numerical and analytical results coincide. The integration of the temperature results in the energy series being $\mathcal{O}(1/\lambda_n^2)$ smaller than that of the temperature, this leads to a much more rapid convergence rate: with $N = 1$ the error is small while with $N = 2$ the series is almost indistinguishable from the numerical result.

If we define

$$E_1(t) = \frac{L^2 C_1 \rho_s c_s}{k_s} \frac{\beta_3 \psi_1(t)}{\lambda_1^4 + \lambda_1^2 \beta_3 (1+\beta_3)} \tag{45}$$

and $E_{\text{app}}(t)$ as the value of E_1 after replacing λ_1 with λ_{app} and then define the relative error

$$\delta(t) = 100 \times \frac{|E_{\text{num}}(t) - E_{\text{app}}(t)|}{|E_{\text{num}}(t)|}\,, \tag{46}$$

we find $\delta(t_f) \approx 1\%$. The error with E_1 is even smaller. Hence we conclude that either equation (45) or E_{app} are sufficiently accurate to describe the energy in a shallow substrate (at least for large times, i.e, close to $t = t_f$). All terms of E_{app} may be written explicitly so this solution provides a significantly more tractable form than the full series which requires the numerical calculation of the eigenvalues. We will verify the accuracy further in the results section.

For the case where we choose constant averaged values to represent the irradiance and ambient temperature, so that $G = 0$ and hence $\mathcal{G}_n = 0$, then

$$\begin{aligned} T_N^0(z,t) =& T_{\text{mn}} + \frac{C_1 L \beta_2}{k} \sum_{n=1}^{N} \left\{ \frac{\cos(\lambda_n)}{\lambda_n^2 + \beta_3 \cos^2(\lambda_n)} \right. \\ & \left. \times \cos\left(\lambda_n \left(1 - \frac{z}{L}\right)\right) \left(1 - \exp\left(-\frac{\lambda_n^2 D_s t}{L^2}\right)\right) \right\}, \end{aligned} \tag{47}$$

which results in a surface temperature and energy

$$T_N^0(0,t) = T_{\text{mn}} + \frac{C_1 L \beta_2}{k} \sum_{n=1}^{N} \frac{1}{\lambda_n^2 + \beta_3^2 + \beta_3} \left(1 - \exp\left(-\frac{\lambda_n^2 D_s t}{L^2}\right)\right), \tag{48}$$

$$\begin{aligned} E_N^0(t) =& \frac{L^2 (C_1 - C_2 T_{\text{mn}})}{D_s} \sum_{n=1}^{N} \left\{ \frac{\beta_3}{\lambda_n^4 + \lambda_n^2 \beta_3 (1+\beta_3)} \right. \\ & \left. \times \left(1 - \exp\left(-\frac{\lambda_n^2 D_s t}{L^2}\right)\right) \right\}. \end{aligned} \tag{49}$$

This solution will be compared later with the thick substrate solution which requires $G = 0$. It is tempting to permit $L \to \infty$ in the above such that the term $1 - \exp(-\lambda_n^2 D_s t / L^2) \to \lambda_n^2 D_s t / L^2$, giving the appearance that for thick layers the surface temperature and energy grow proportional to time, so contradicting the previous deep substrate results. However this naive expansion does not capture the correct behaviour since $\beta_3 \to \infty$ and $\lambda_n \to \sqrt{\beta_3}$ (independent of n) as $L \to \infty$.

In Figure 5 (a) we show a comparison of the surface temperature predicted by the separable solution, (48), with $N = 100$, $L = 10, 15$ cm, and that obtained for an infinite depth substrate (30). Here it becomes clear that as L increases the separable solution approaches the infinite depth solution. All solutions in the figure have $G(t) = 0$, that is the temperature and irradiance are set to their average values. For this reason the surface temperature steadily increases during the day, in contrast to the result presented earlier in Figure 4, which has a variable energy input. For $L = 15$ cm the results are virtually identical for the whole day whereas for $L = 10$ cm they start to diverge after around 6 hours (when $\lambda_n^2 D_s t/L^2$ becomes $\mathcal{O}(1)$). The corresponding energy stored in the layer is presented in Figure 5 (b), but now we only take two terms in the series solution. The nonlinear behaviour is apparent. Again, as the depth of the substrate increases the series solution approaches that of the Laplace solution, with an error of approximately 4% at the end of the day when $L = 15$cm.

3.3. Method to determine the amount evaporated, $d(\alpha)$

Evaporation plays a key role in the absorption and storage of energy. It is one of the main reasons why a dark soil surface can remain cooler than a lighter concrete one: evaporation requires a lot of energy. Here we have taken a standard approximation by setting the evaporation rate proportional to the surface temperature, $\dot{d} = \alpha T(0, t)$. However, the constant of proportionality, which determines the energy loss term C_2, is *a priori* unknown and must be calculated during the solution process.

In the case where the evaporation rate is assumed to be constant the solution is simple. Writing $\dot{d} = d/t_f$, where it is assumed that the liquid evaporated during the day, d, is a known depth, then α may be removed from the problem. The constants C_1, C_2 take on a slightly different definition

$$C_1 = (1 - F_{VC})(1 - A_s)Q_{av} + H_{as}T_{av} - \rho_w L_e \frac{d}{t_f}\,, \quad C_2 = H_{as}\,. \tag{50}$$

These different definitions do not affect the previous calculations, so the expressions derived in the preceding sections for temperature and energy absorbed still hold but with C_1, C_2 defined by (50).

In the more physically realistic situation, where evaporation varies through the day the constants are as defined in (20) and α may be determined by integrating the derived expression for $T(0, t)$ and employing equation (22) or

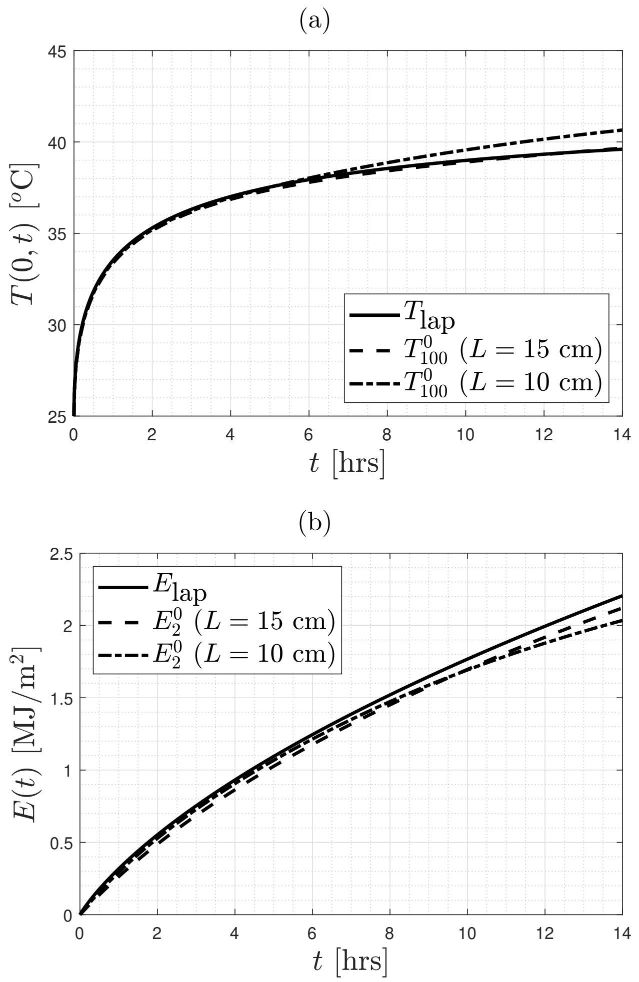

Figure 5: Comparison of separable (48) and Laplace (30) solutions for the surface temperature and energy when $G(t) = 0$ for $L = 10, 15$cm: (a) Surface temperature taking $N = 100$ (b) Stored energy taking $N = 2$.

by equating the energy expression with the result of equation (27). For the case of a thick layer setting $t = t_f$ in (31) and equating the result with (27) we obtain

$$\begin{aligned} d =& \frac{\alpha}{C_2}\left[C_1 t_f - \frac{k_s\rho_s c_s}{C_2^2}(C_1 - C_2 T_{\text{mn}}) \right. \\ &\left. \times \left(\exp\left(\frac{C_2^2 D_s}{k_s^2} t_f\right)\text{erfc}\left(\frac{C_2}{k_s}\sqrt{D_s t_f}\right) + \frac{2}{\sqrt{\pi}}\frac{C_2}{k_s}\sqrt{D_s t_f} - 1\right)\right], \end{aligned} \tag{51}$$

For thinner layers, setting $t = t_f$ in (44) and equating with (27) we obtain

$$d = \frac{\alpha C_1}{C_2}\left[t_f - \frac{L^2 \rho_s c_s}{k_s}\sum_{n=1}^{\infty}\frac{\beta_3 \psi_n(t_f)}{\lambda_n^4 + \lambda_n^2 \beta_3(1+\beta_3)}\right], \tag{52}$$

where λ_n is obtained by solving (36) and $\psi_n(t_f)$ given explicitly by (37).

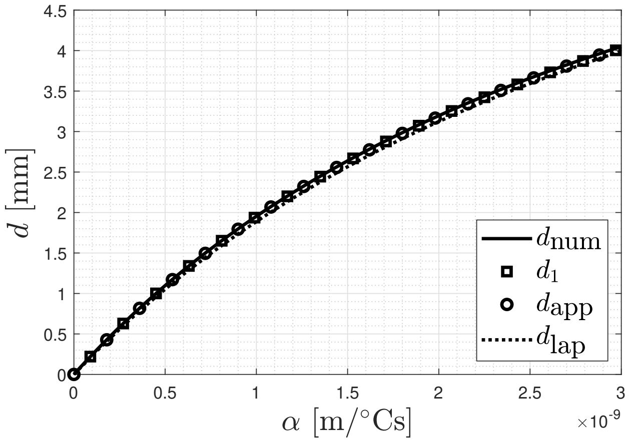

Figure 6: Depth evaporated as a function of α, for $L = 8$cm, obtained by numerical integration, d_{num}, the solution of (52) using only the first term with the exact value of λ_1, denoted d_1, and using the first term with the approximate value of λ_1, denoted d_{app}, and the solution of (51), denoted d_{lap}

In Figure 6 we show the depth of water evaporated as a function of α using infinite and finite depth solutions, (51, 52). Having demonstrated that the energy converges rapidly and that $E_1(t_f)$ agrees very well with the full numerical solution for the finite depth we only use the first term of the finite depth solution which defines

$$d_1 = \frac{\alpha C_1}{C_2}\left[t_f - \frac{L^2 \rho_s c_s}{k_s}\frac{\beta_3 \psi_1(t_f)}{\lambda_1^4 + \lambda_1^2 \beta_3(1+\beta_3)}\right]. \tag{53}$$

Taking the exact value of λ_1, determined by solving $\lambda_1 \tan \lambda_1 = \beta_3$ numerically, we obtain the curve labelled d_1. Using the approximate expression for the first eigenvalue, (42), gives d_{app}. Also shown is the numerical solution of the heat equation. In all cases we take $L = 8$cm and parameter values specified in the following section. Clearly the agreement between the four forms is excellent. In each case the depth increases non-linearly with α. Although calculated with $L = 8$cm we found virtually identical results for larger values, such that for sufficiently thick layers we may assume that $d(\alpha)$ is independent of depth. This may be attributed to the fact that evaporation is a surface effect. Here affecting a maximum of approximately 4.5mm into the soil layer. The soil far below this, such that $L \gg 4.5$mm will have little influence on this process. From the deep substrate result (51) we know that d depends linearly on C_1. From Fig. 6 it is clear that the computed value of d is almost identical for both shallow and deep layers. As a consequence the energy absorbed, expressed by (27), is linear in C_1 for any depth of substrate (greater than a few millimetres). This means that the energy decreases linearly with fractional leaf coverage F_{VC}, albedo, A_s, and increases linearly with irradiance Q_{net} and average daily temperature. The nonlinear dependence of both expressions on C_2 shows that $E(t_f)$ depends nonlinearly on the evaporation rate and heat transfer coefficient. This will be demonstrated in §4.3.

4. Results

After developing a set of solutions appropriate for thick and thin substrates the goal is now to see how they behave under realistic conditions and in doing so determine guidelines or advice concerning the design of green roofs.

The thermophysical properties of soils vary significantly depending on the composition and moisture content. Coma *et al.* [36] analysed the properties of five different dried soils for extensive green roofs, changing the percentage of compost, coco peat, crushed building wastes, coarse grained sand and pozzolana, to obtain $k_s \in [0.1, 0.19]$ W/m°C, $c_s \in [724, 873]$ J/kg°C, $\rho_s \in [375, 1360]$ kg/m^3. In [37] the soil layer has the following properties: $k_s =$ 0.27 W/m°C, $c_s =$ 1307 J/kg°C, $\rho_s =$ 1210 kg/m^3, the layer thickness was $L = 8\,$cm and the albedo $A_s = 0.26$. We will use this latter soil as a reference case and choose a fractional vegetative cover of $F_{VC} = 0.5$.

The typical properties of concrete used in construction may also vary with composition. For example, the density of regular concrete is around 2400 kg/m^3 while lightweight concrete has $\rho_c \approx 1750$ kg/m^3 [38]. In our subsequent analysis, we will use parameter values consistent with HSC concrete as presented in Table 2 [39, 40]. With regard to the ambient conditions, unless otherwise specified, we will use the parameter values given in Table 3, which are consistent with a roof in a city with warm but not extreme temperatures and with a medium irradiance.

4.1. Temperature and energy profiles

In this section we focus on a green roof using the data provided in Tables 2, 3 and $A_s = 0.26$, $L = 8$cm unless specified otherwise. The numerical solution of the heat equation (1) subject to (19) is used to determine the temperature at the soil-air interface and the energy stored as a function of time in Figure

Table 2: Representative values for the thermophysical properties of soil and concrete [37, 38, 40, 41].

Material	ρ_i (kg/m^3)	c_i (J/kg°C)	k_i (W/m°C)
soil (i=s)	1210	1307	0.27
concrete (i=c)	2300	1000	1.5

Table 3: Parameters used to represent ambient conditions, values for H_{as} and $Q_{\max}$ are taken from [42], [43] respectively.

Maximum temperature	$T_{\max}$	30	°C
Minimum temperature	$T_{\min}$	20	°C
Maximum irradiance	$Q_{\max}$	800	W/m^2
Density of water	ρ_w	1000	kg/m^3
Soil-air heat transfer coefficient	H_{as}	5	W/m^2°C
Latent heat of evaporation	L_e	2.26×10^6	J/kg

7. The left panel shows the evolution of the surface temperature for different thicknesses while the right one corresponds to the evolution of the absorbed energy. The surface temperature is always highest with the thinnest layer, reaching a maximum of approximately 52°C soon after midday (which occurs at $t = 7$ hours). As the layer thickness increases the surface temperature decreases, since the heat can diffuse further into the layer. The two plots for $L = 13, 15$cm are difficult to distinguish, suggesting that for $L > 15$cm the surface temperature is independent of depth (and hence the infinite depth solution will be accurate). The higher surface temperature results in a higher evaporation rate and convective cooling and for this reason less energy is retained in the thinner soil layer. Consequently, in contrast to the surface temperature, the energy stored is greater in the thicker layers, attaining a maximum of around 2.4 MJ/m^2 when $L = 15$cm while for the 5cm layer the maximum is close to 2 MJ/m^2. Thicker layers clearly have the ability to store more energy whilst maintaining a lower surface temperature.

4.2. Effect of evaporation

In Figure 8 we plot the energy at the end of the day as a function of the evaporated depth as predicted by integrating the numerical solution for the full problem via equation (23) with $G \neq 0$, denoted $E_{\text{num}}(t_f)$, and with the average values (hence $G = 0$), $E^0_{\text{num}}(t_f)$. Also shown are the analytical solutions, the Laplace solution, (31), $E_{\text{lap}}(t_f)$, which has $G = 0$ and the approximate separable solution E_{app}, which has $N = 1$ and $\lambda_1 = \lambda_{\text{app}}$. As discussed earlier the energy decreases linearly with d, due to the increasing

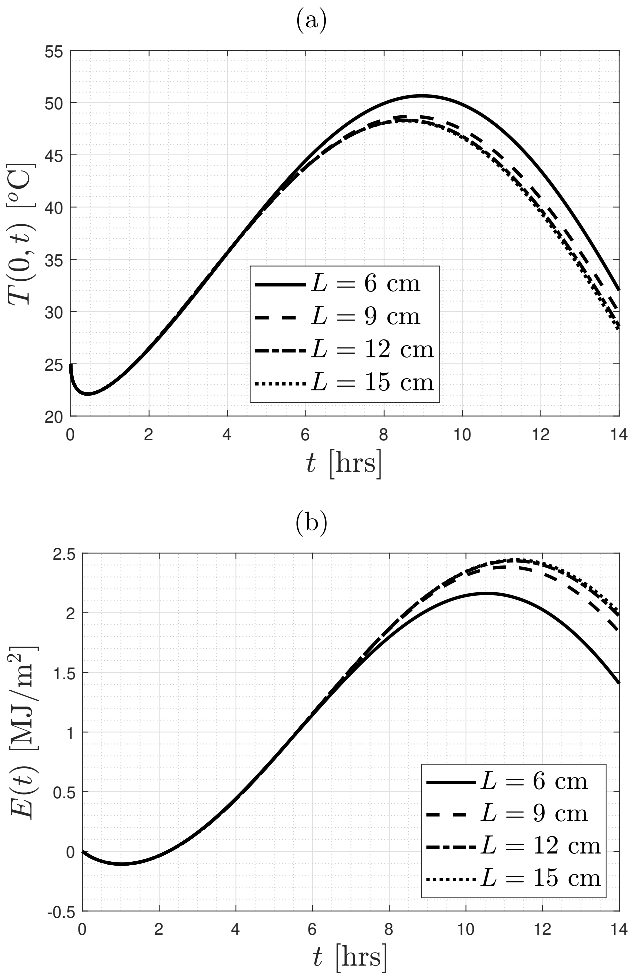

Figure 7: Numerical solutions for (a) Evolution of the temperature at the air-soil surface for different soil thicknesses, (b) Evolution of the energy for different soil thicknesses. In both cases $\alpha = 1$ nm/°Cs.

energy removed by evaporation. In Figure 8(a) the Laplace solution provides a poor approximation, indicating that this substrate is too shallow for the infinite layer analysis. The approximate solution E_{app} shows good agreement with the full numerical solution, demonstrating that the behaviour is well captured by this simple explicit representation. The numerical solution with $G = 0$ shows an error of approximately 3% which results from neglecting the variation in ambient temperature and irradiance. Increasing the substrate depth to 15cm on Figure 8(b) it may be seen that the Laplace solution now becomes accurate, within the assumption of $G = 0$: the agreement with E^0_{num} is excellent. Surprisingly E_{app} also appears to closely match these

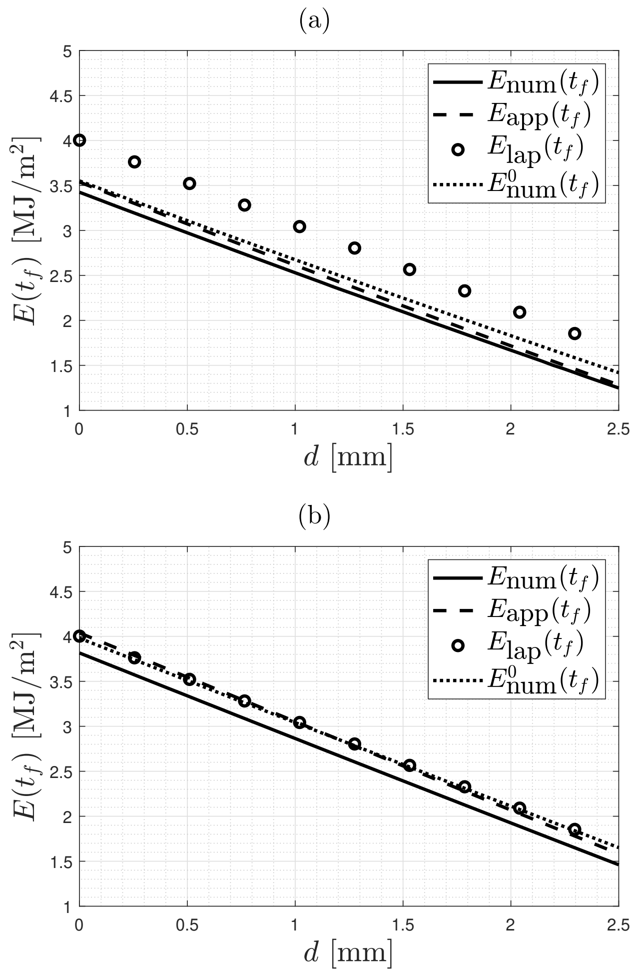

Figure 8: Energy absorbed at the end of the day using the numerical solution of the heat equation and expression (23) with $G \neq 0$, denoted $E_{\text{num}}(t_f)$, and with $G = 0$, denoted $E^0_{\text{num}}(t_f)$, also shown are (45) for E_{app} and (31) for $E_{\text{lap}}(t_f)$: (a) Soil thickness of $L = 8$cm. (b) Soil thickness of $L = 15$cm.

two solutions. The distance from the full numerical solution is a result of the approximation to λ_1 which becomes worse with increasing depth, for $L = 15$cm the error in λ_1 is of the order 9% but this only results in an error for the energy prediction of approximately 5%.

4.3. Albedo and vegetative cover effects

The albedo and the fractional vegetative cover are properties which directly affect the amount of solar irradiance reaching the surface and consequently must play a strong role in the energy storage. As discussed in §3.3 for a thick layer the energy absorbed varies linearly with C_1 and so must decrease linearly with increasing F_{VC} and A_s. For a thin layer the dependence is not clear from the analytical solution but the fact that the deep and shallow results coincide for the depth $d(\alpha)$ suggests a linear decrease with C_1. In Figure 9 we show the dependence of the total energy as a function of the fractional vegetative cover F_{VC} when $L = 8$cm and with various evaporation rates. The linear decrease is apparent in all cases, even though the layer is not sufficiently thick to warrant applying the infinite thickness solution. As we increase the vegetative cover to unity, with $\alpha = 0$ (that is no evaporation), the stored energy becomes very small. This is to be expected, there is no incoming irradiance so energy only passes to the substrate through convective heat transfer which is much less efficient. Increasing the amount evaporated the energy at the end of the day can become negative, that is there is less energy in the substrate than at the beginning of the day. This demonstrates the strong effect evaporation can have on the process. Since the incoming energy depends on $(1 - F_{VC})(1 - A_s)Q_{\text{net}}$ exactly the same behaviour can be expected by fixing F_{VC} and varying the albedo. Consequently Figure 9 also holds for varying $A_s \in [0, 1]$ with fixed F_{VC}.

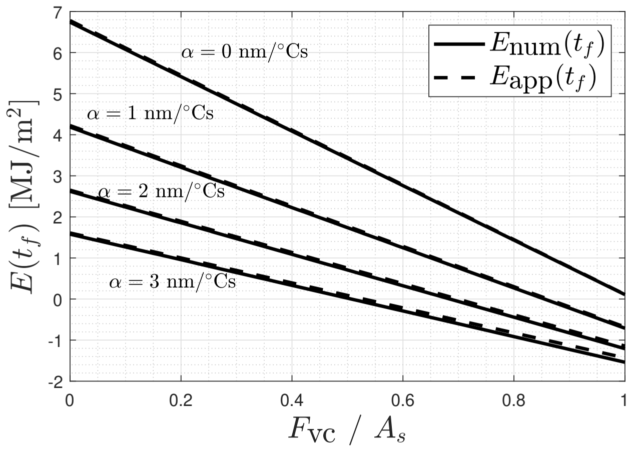

Figure 9: Total energy stored as a function of F_{VC} or A_s using direct numerical simulation and the approximate expression (45) for different values of α.

4.4. Surface temperature and energy stored in concrete layers

The model is easily applied to a concrete or other man-made surface by setting $F_{VC} = d = 0$ in all expressions. Thermophysical parameters are shown in Table 2 and typical values for the albedo are shown in Table 4: unpainted concrete has values between 0.2 and 0.45. In Figure 10(a) we show the surface temperature with $A_c = 0.3$ for three different concrete layer thicknesses. As before the thinner layers show a higher value. In

Table 4: Typical albedo values for different types of surfaces.

Material	Albedo	Reference
concrete	0.2-0.45	[44–46]
asphalt	0.05-0.20	[45, 46]
brick, stone	0.20–0.40	[46]
sandy soil	0.25-0.45	[47]
bare fields	0.1-0.25	[47]
grass, bushes	0.16-0.27	[37, 43, 47]
trees	0.15-0.18	[46]
white paint	0.5-0.9	[46]
black paint	0.05	[48]

order to compare with a green roof, we also show the equivalent result taken from Figure 7(a). For the 6cm layer the maximum difference in surface temperatures between green and concrete roofs is close to 40°C. Even for the 12cm layer the difference is of the order 30°C. This clearly demonstrates how green roofs can affect comfort levels. Figure 10(b) shows the energy stored in a concrete roof for $L \in [6, 16]$cm when $A_c = 0.3$, we also present a second result corresponding to using a reflective paint, with $A_c = 0.7$. The corresponding green roof result is shown as a solid line. With the unpainted surface the energy stored ranges between four to six times that in a typical green roof. Even with the reflective coating the energy stored is typically twice that of the green roof. All this extra energy is available for release during the night and so will add to the heat island effect.

4.5. Comparison between intensive and extensive green roofs

The key difference between intensive and extensive green roofs is the depth of the substrate. Extensive roofs typically have a substrate between approximately 5-12cm while intensive roofs are deeper.

The deeper growing medium of an intensive roof permits a wide range of plant types, ranging from grasses to shrubs or even trees. These large plants provide a lot of shade on the soil, so their mean leaf area index (LAI) ranges from 1 to 6 or even 7 (see [49]), and they have been found to have albedo values ranging from 0.16 to 0.28 (see [50]).

Extensive green roofs typically allow for hardy plants which require minimum maintenance. Since these plants are typically smaller, so are their leaves and they usually require little watering. Extensive roofs are usually "browner", so their albedo is low. Since plants of extensive green roofs are typically grass or have small leaves, their LAI is also small, ranging from 0.8 to 2.

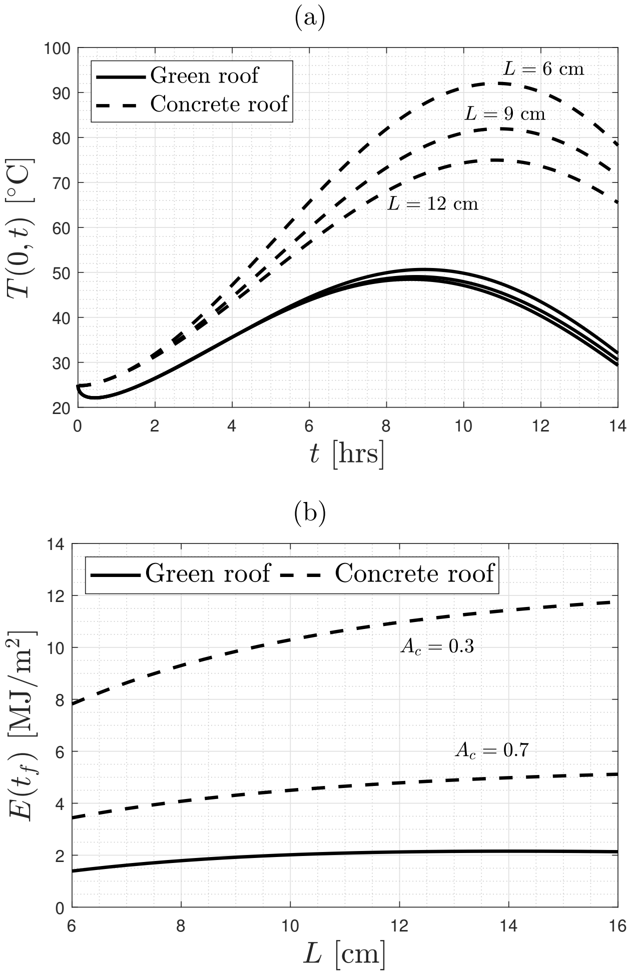

Figure 10: (a) Surface temperature for a concrete and green roofs using direct numerical simulation. Albedo value for concrete used here is $A_c = 0.3$. Curves relative to green roofs are plotted for comparative purposes, we suggest observing Figure 7(a) for a better reference. (b) Total energy stored at the end of the day. The different albedo values correspond to unpainted ($A_c = 0.3$) and painted ($A_c = 0.7$) concrete.

These two types of green roofs are dramatically different in terms of maintenance, leading to the natural question whether it is worth investing in a more sophisticated "rooftop garden" rather than simply providing a shallow layer of soil with small vegetation. We therefore now use our model and consider two different set of values for the albedo and the vegetative coverage and compare the total energy stored in the two cases as a function of the soil thickness. We will consider a range of values in the two cases.

Table 5 shows the values used in the numerical simulations. The rest of the parameters are kept the same as in the previous sections.

Table 5: Representative values for intensive and extensive green roofs [49, 50].

Type of roof	A	LAI	F_{VC}	L (cm)
Intensive	0.26	2.5	0.92	12-20
Extensive	0.20	1	0.63	5-12

Figure 11 shows the evolution of $E(t)$ over the day for the two roof types. We recall that our models are valid for small evapotranspiration rates and root uptake. The predictions should therefore be treated with caution when dealing with large plants, for this reason we use a moderate value for the LAI in the intensive case. The curves were obtained by numerically computing the evolution of the energy absorbed during the day for a range of soil thicknesses and then calculating the mean energy for each range. For extensive roofs we used 5-10.5cm, whereas for the intensive ones we used 12-20cm (as shown in Fig. 10b) the energy shows only a weak depth dependence in these ranges). In this case the total stored energy at the end of the day for extensive green roofs is around 1.5 MJ/m^2. For the intensive green roof a negative value, around -0.4 MJ/m^2, is obtained. The negative value indicates that energy has been lost during the day, so highlighting the significant advantage of intensive over extensive roofs.

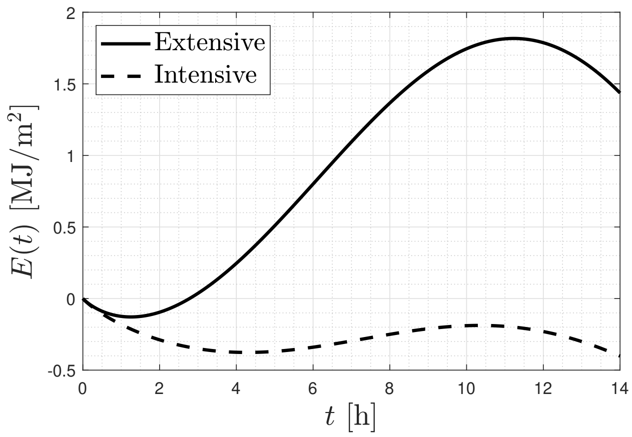

Figure 11: Time evolution of the absorbed energy for intensive and extensive green roofs.

4.6. Non-insulated soil bottom

In the original model, the boundary conditions at the bottom of the soil represent two possible scenarios: either the temperature there remains at the initial temperature during the whole day or there is no heat transfer from the soil to the building. In practice, we may wish to extend the second case and assume that a certain amount of heat is lost into the building. This requires modifying the boundary condition at $z = L$ to

$$-k_s \frac{\partial T}{\partial z}\bigg|_{z=L} = \epsilon C_1, \quad \epsilon > 0\,. \tag{54}$$

This form indicates that the heat lost at the base is proportional to that input at the surface, represented by C_1. The constant of proportionality, $\epsilon > 0$, is expected to be small and in the limit $\epsilon \to 0$ the insulated boundary condition is retrieved. Imposing (54) the temperature can be expressed in the form of equation (35), although now the expression for ψ_n is

$$\psi_n(t;\epsilon) = \left(\beta_2 - \frac{\epsilon}{\cos(\lambda_n)}\right)\left[1 - \exp\left(-\frac{\lambda_n^2 D_s t}{L^2}\right)\right] + \lambda_n^2 \mathcal{G}_n(t)\,, \tag{55}$$

see Appendix A for the detailed procedure. In particular, we note that equation (55) reduces to (37) in the limit $\epsilon \to 0$.

In Fig. 12 we show the effect of the parameter ϵ on the surface temperature and the amount of energy stored during the day for a green roof with $L = 8$cm. The temperature is truncated after 100 terms, the energy after 2 terms (these results are almost identical to the numerical solution). From Fig. 12a) it is apparent that the substrate heat loss has little impact on the surface temperature, which is dominated by surface effects. Since energy is now being lost at the bottom of the substrate ϵ has a much stronger influence on the absorbed energy, which decreases by around 15% at the end of the day as ϵ increases from 0 to 10, as shown in Fig. 12b).

To estimate a typical value for ϵ we consider a situation where there is a room with temperature $T_{room} = 25\,^o$C located at $z = L$, i.e. directly below the green roof. The right hand side of Eq. (54) represents the heat flux flowing into the room through the ceiling, which can be expressed as $q_{room} = H_{cr}(T_{ceiling} - T_{room})$ where H_{cr} is the ceiling-room heat transfer coefficient and $T_{ceiling}$ is the temperature of the ceiling. Heat transfer coefficients between indoor air and ceilings in regular buildings have values around $5\,\mathrm{W/m^2\,^oC}$ or smaller [51, 52]. To obtain an upper bound for ϵ we assume that the temperature of the ceiling takes a very high value $T_{ceiling} = \max\left[T(z=0,t)\right]$ where $T(z = 0, t)$ is the temperature at the roof surface for the insulated case (in practice $T_{ceiling}$ would be much lower than the surface temperature). Combining the expression for q_{room} with the right hand side of Eq. (54) shows $\epsilon = H_{cr}(T_{ceiling} - T_{room})/C_1$. Using the results for both green and concrete roofs with $L = 6$ cm as shown in Fig. 10, we have $T^{GR}_{ceiling} = 50.65\,^o$C,

(a)

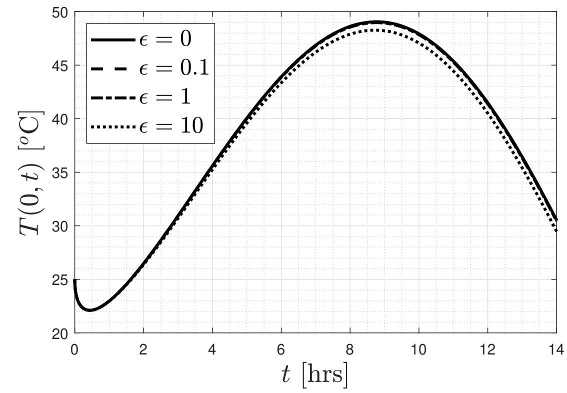

(b)

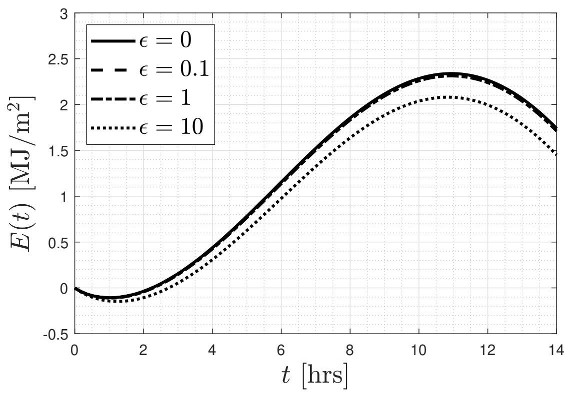

Figure 12: Evolution of (a) surface temperature and (b) stored energy for different values of the heat loss parameter ϵ. In both cases $L = 8$cm, $\alpha = 1$nm/°Cs.

$C_1^{GR} = 315.9$ and $T_{ceiling}^{concrete} = 92.03\,^o$C, $C_1^{concrete} = 483.97$. These values lead to $\epsilon^{GR} = 0.41$ and $\epsilon^{concrete} = 0.69$, respectively. So, even in the $L = 6\,$cm case which has the highest temperature of our calculations and with no heat loss through the layer, the upper bound has $\epsilon < 1$. Referring to Fig. 12 which shows negligible differences between the $\epsilon = 0$ and $\epsilon = 1$ cases we may conclude that the insulating boundary condition is sufficient for all practical purposes.

5. Conclusions

The primary aims of this paper were to develop a mathematical model for heat flow in a green roof, to develop analytical solutions and to use these to gain a better understanding of the process and finally, to evaluate the differences in energy storage between green and concrete or man-made roofs. The intention being that such a model could provide simple guidelines with regard to the design of green roofs.

Various analytical solutions were presented, which explicitly define the role of system parameters. A numerical solution was also developed this permitted verification of the analytical solutions but could not clarify the role of individual parameters. For an infinitely thick substrate an analytical expression was presented, provided that the daily variation of ambient temperature and irradiance is averaged. For large time, close to the end of the day, this solution demonstrated a simple linear dependence of the energy on many of the ambient conditions, while the energy varied with the square root of time and thermophysical properties of the substrate. For finite thickness layers a separable solution was found. The energy expression converged rapidly at large times and so could be written in an explicit form, involving only the first term, which again permits the role of ambient conditions to be clearly understood.

Comparison between the analytical solutions and the numerical solution demonstrated that:

1. The separable solution for the energy rapidly converges such that by the end of the day only a single term is required. The surface temperature converges much more slowly.
2. The infinite depth solution holds for substrates deeper than approximately 15cm.
3. The averaging of the ambient temperature and irradiance results in slightly higher predictions for energy absorption, but the trend is the same as the numerical solution of the full, time-dependent system.

Given that the majority of green roofs have a depth greater than 15cm this final point suggests that the Laplace solution provides a simple way to quantify the energy storage.

Significant conclusions from the model include:

1. Subject to identical conditions, e.g. the same albedo, solar radiation, vegetative coverage etc, an extensive (thin layer) green roof will exhibit higher surface temperatures than an intensive (thick) roof but will absorb less energy. However, in practice an intensive roof typically has the higher vegetative coverage and albedo. In which case intensive

roofs absorb significantly less energy and so, whenever possible, are preferable to extensive roofs.

2. Concrete roofs are significantly hotter and store significantly more energy than a standard green roof. Our example showed a maximum surface temperature almost 40°C higher and a factor three more energy stored between concrete and green roofs.

If the energy stored in a green roof is a factor x less than that in an equivalent concrete layer then we may easily deduce that a 10% increase in an area's green coverage corresponds to a $10(x-1)/x$ % decrease in stored energy. For the present example $x \approx 3$ which corresponds to a 6.7% decrease in energy stored for every extra 10% of green area.

With regards to guidelines to aid in the design of green roofs, within the restrictions of the present model, the results show that the energy absorbed:

1. Decreases linearly with: depth of water evaporated; fractional vegetative coverage; albedo.
2. Increases linearly with average ambient temperature.
3. Varies non-linearly with surface temperature (related to the evaporation rate) and the surface heat transfer coefficient.
4. Increases with the square root of the thermophysical properties such as density of the soil, thermal conductivity and specific heat capacity.

Obviously not all of these may be controlled but ensuring good leaf coverage, a lighter coloured surface and a wet surface layer are possible. These are the most important factors. Choosing a substrate with a low density, conductivity and heat capacity will, to a lesser extent, reduce the energy storage capacity.

While there exist many more complex descriptions of heat flow in urban landscapes, including detailed descriptions of air flow and energy input from human activity it is imperative that these models are founded on the correct building block. The current model is designed to achieve this. It may be adapted to incorporate empirical modifications, such as those employed in the Penman-Monteith equation where, for example, the surface heat transfer accounts for the air speed some distance above the ground, or the evaporation is split into evaporation and transpiration. However, swapping the heat transfer coefficient for an air speed expression or removing liquid from inside the soil layer as well as at the surface will not change the basic conclusions. Other modifications, which can add to the generality of the model include permitting heat transfer between the green roof and the building surface, so paving the way to study the effect inside the building, and also permitting moisture movement within the soil.

Author Statement

The work has not been published previously and it is not under consideration for publication elsewhere. Its publication is approved by all authors. If accepted, it will not be published elsewhere in the same form, in English or in any other language, including electronically without the written consent of the copyright-holder.

Declaration of Competing Interest

All authors have participated in (a) conception and design, or analysis and interpretation of the data; (b) drafting the article or revising it critically for important intellectual content; and (c) approval of the final version. This manuscript has not been submitted to, nor is under review at, another journal or other publishing venue. The authors have no affiliation with any organization with a direct or indirect financial interest in the subject matter discussed in the manuscript.

CRediT authorship contribution statement

Maria Aguareles: Conceptualization, Methodology, Formal analysis, Writing - original draft, Software. **Marc Calvo-Schwarzwalder:** Formal analysis, Writing - review & editing. **Francesc Font:** Conceptualization, Methodology, Formal analysis, Writing - original draft, Software. **Timothy G. Myers:** Supervision, Conceptualization, Writing - review & editing.

Acknowledgements

M. Aguareles acknowledges grant no. MTM2017-84214-C2-2-P. M.Calvo-Schwarzwalder acknowledges financial support from Zayed University through the grant no. R21033 and the Policy Research Incentive Program 2022. F. Font acknowledges the support of the Serra-Hunter Programme of the Generalitat de Catalunya. T.G. Myers thanks the CERCA Programme of the Generalitat de Catalunya. All authors acknowledge the support of Ministerio de Ciencia e Innovación Grant No. PID2020-115023RB-I00.

Appendix A. Temperature profile for infinite depth substrate

The model presented in this work can be solved analytically if we assume that

1. the air temperature and sun irradiation remain constant along the day;

2. the thickness of the soil can be assumed to be infinite.

Under these conditions, the governing equations are

$$\frac{\partial T}{\partial t} = D_s \frac{\partial^2 T}{\partial z^2}\,, \qquad T(z,0) = T_{\mathrm{mn}}\,, \tag{A.1a}$$

$$-k_s \frac{\partial T}{\partial z}\bigg|_{z=0} = C_1 - C_2 T(0,t)\,, \qquad \frac{\partial T}{\partial z}\bigg|_{z\to\infty} = 0\,. \tag{A.1b}$$

To simplify notation and to understand the contributions and relative importance of the different terms in the equations, it is helpful to formulate the problem first in terms of scaled variables. The arising dimensionless numbers can then yield some interesting behaviour of the solutions.

Appendix A.1. Non-dimensional formulation

For the problem defined by (A.1) there is a clearly defined time scale t_f. The length and temperature scales can be determined by writing $z = \mathcal{L}\hat{z}$, $t = t_f\hat{t}$ and $T = T_{\mathrm{mn}} + \mathcal{T}\hat{T}$, which leads to

$$\frac{\partial \hat{T}}{\partial \hat{t}} = \frac{\partial^2 \hat{T}}{\partial \hat{z}^2}\,, \qquad \hat{T}(\hat{z},0) = 0\,, \qquad \frac{\partial \hat{T}}{\partial \hat{z}}\bigg|_{\hat{z}\to\infty} = 0\,, \tag{A.2}$$

provided we choose $\mathcal{L} = \sqrt{t_f/D_s}$. The boundary condition at the surface reads

$$-\frac{k_s \mathcal{T}}{\mathcal{L}} \frac{\partial \hat{T}}{\partial \hat{z}}\bigg|_{\hat{z}=0} = C_1 - C_2 T_{\mathrm{mn}} - C_2 \mathcal{T}\hat{T}(0,\hat{t})\,. \tag{A.3}$$

Upon choosing the temperature scale $\mathcal{T} = C_1\mathcal{L}/k_s$, this condition reduces to

$$-\frac{\partial \hat{T}}{\partial \hat{z}}\bigg|_{\hat{z}=0} = \beta_2 - \beta_3 \hat{T}(0,\hat{t})\,, \tag{A.4}$$

where

$$\beta_2 = 1 - \frac{C_2 T_{\mathrm{mn}}}{C_1}\,, \qquad \beta_3 = \frac{C_2 \mathcal{L}}{k_s}\,. \tag{A.5}$$

Appendix A.2. Analytical solution

Taking the Laplace transform of the system defined by Eqs. (A.2) and (A.4) we obtain

$$\hat{s}\hat{u} = \frac{\partial^2 \hat{u}}{\partial \hat{z}^2}, \qquad \hat{u}\,(\hat{z},0) = 0\,, \tag{A.6a}$$

$$-\frac{\partial \hat{u}}{\partial \hat{z}}\bigg|_{\hat{z}=0} = \frac{\beta_2}{s} - \beta_3 \hat{u}\,(0,\hat{s}) \qquad \frac{\partial \hat{u}}{\partial \hat{z}}\bigg|_{\hat{z}\to\infty} = 0, \tag{A.6b}$$

where $\hat{u}\left(\hat{z}, \hat{s}\right)$ is the Laplace transform of $\hat{T}\left(\hat{z}, \hat{t}\right)$. The solution to the ordinary differential equation is

$$\hat{u}\left(\hat{z}, \hat{s}\right) = A \exp\left(-\sqrt{\hat{s}}\hat{z}\right) , \tag{A.7}$$

where the positive branch has been neglected to satisfy the far-field condition. Applying the boundary condition at $\hat{z} = 0$ determines

$$A = \frac{\beta_2}{\hat{s}(\beta_3 + \sqrt{\hat{s}})} , \tag{A.8}$$

and hence we can transform back to obtain

$$\begin{aligned}\hat{T}\left(\hat{z}, \hat{t}\right) =& \frac{\beta_2}{\beta_3}\left[\operatorname{erfc}\left(\frac{\hat{z}}{2\sqrt{\hat{t}}}\right)\right. \\ &\left.- \exp\left(\beta_3\left(\beta_3 \hat{t} + \hat{z}\right)\right) \operatorname{erfc}\left(\beta_3\sqrt{\hat{t}} + \frac{\hat{z}}{2\sqrt{\hat{t}}}\right)\right] ,\end{aligned} \tag{A.9}$$

where $\operatorname{erfc}(z)$ is the complementary error function,

$$\operatorname{erfc}(z) = \frac{2}{\sqrt{\pi}} \int_z^\infty e^{-t^2}\, \mathrm{d}t \,.$$

In the original variables, the temperature reads

$$\begin{aligned}T(z,t) =& T_{\mathrm{mn}} + \frac{C_1 - C_2 T_{\mathrm{mn}}}{C_2}\left[\operatorname{erfc}\left(\frac{z}{2\sqrt{D_s t}}\right)\right. \\ &\left.- \exp\left(\frac{C_2}{k_s}\left(\frac{C_2 D_s t}{k_s} + z\right)\right) \operatorname{erfc}\left(\frac{z}{2\sqrt{D_s t}} + \frac{C_2\sqrt{D_s t}}{k_s}\right)\right] .\end{aligned} \tag{A.10}$$

Appendix A.3. Total energy absorbed

We can rewrite the energy in terms of the non-dimensional variables,

$$E(t) = \rho_s c_s \mathcal{L}\mathcal{T} \int_0^\infty \hat{T}\left(\hat{z}, t/t_f\right) \mathrm{d}\hat{z} \,, \tag{A.11}$$

which requires the results

$$\begin{aligned}\int_0^\infty \operatorname{erfc}\left(\frac{z}{a}\right)\, \mathrm{d}z =& a\left[z \cdot \operatorname{erfc}\left(\frac{z}{a}\right) - \frac{1}{\sqrt{\pi}} \exp\left(-\frac{z^2}{a^2}\right)\right]_0^\infty \\ =& \frac{a}{\sqrt{\pi}} ,\end{aligned} \tag{A.12}$$

$$\begin{aligned}\int_0^\infty \exp(bz)\operatorname{erfc}\left(\frac{ab}{2} + \frac{z}{a}\right)\, \mathrm{d}z =& \frac{1}{b}\left[\exp(bz)\operatorname{erfc}\left(\frac{ab}{2} + \frac{z}{a}\right)\right. \\ &\left. + \exp\left(-\frac{a^2}{4b^2}\right) \operatorname{erf}\left(\frac{z}{a}\right)\right]_0^\infty \\ =& \frac{1}{b}\left[\exp\left(-\frac{a^2}{4b^2}\right) - \operatorname{erfc}\left(\frac{ab}{2}\right)\right] ,\end{aligned} \tag{A.13}$$

where $a = 2\sqrt{D_s t}$ and $b = C_2/k_s$. In the original dimensional variables, the absorbed energy is

$$\begin{aligned} E(t) = & \frac{k_s^2}{D_s C_2^2}(C_1 - C_2 T_{\text{mn}}) \left[\exp\left(\frac{C_2^2 D_s}{k_s^2} t\right) \operatorname{erfc}\left(\frac{C_2}{k_s}\sqrt{D_s t}\right) \right. \\ & \left. + \frac{2}{\sqrt{\pi}} \frac{C_2}{k_s} \sqrt{D_s t} - 1 \right] . \end{aligned} \tag{A.14}$$

Appendix B. Derivation of the temperature for a finite substrate with varying Q_{net} and T_a

In the case where the environmental conditions are not assumed constant, the problem is impossible to solve analytically and numerical and approximate solutions are required. Whereas numerical solutions are useful to rapidly visualise the solution to specific problems, explicit solutions allow a better understanding of the role of the different parameters of the problem. Here we derive a solution based on a generalised eigenfunction expansion, which is always a valid method when the equations are linear.

In a soil with a finite length L and with varying environmental conditions, the governing equations are

$$\frac{\partial T}{\partial t} = D_s \frac{\partial^2 T}{\partial z^2}\,, \qquad T(z,0) = T_{\text{mn}}\,, \tag{B.1a}$$

$$-k_s \left.\frac{\partial T}{\partial z}\right|_{z=0} = C_1 + G(t) - C_2 T(0,t)\,, \qquad \left.\frac{\partial T}{\partial z}\right|_{z=L} = 0\,, \tag{B.1b}$$

where $C_1 = (1 - F_{VC})(1 - A_s)Q_{\text{av}} + H_{as}T_{\text{av}}$, $C_2 = H_{as} + \rho_w L_e \alpha$ and $G(t)$ is defined by

$$G(t) = (1 - F_{VC})(1 - A_s)Q_{\text{net}}(t) + H_{as}T_{\text{a}}(t)\,. \tag{B.2}$$

Similarly to the case of infinite depth solved in Appendix A, we will first reformulate the problem in terms of scaled variables. Additionally to the non-dimensional numbers arising in the case of the infinitely deep soil, in this case we have an additional parameter relative to the varying environmental conditions.

Appendix B.1. Non-dimensional formulation

The thickness of the soil L provides the length scale to this problem, which has an associated diffusion time scale L^2/D_s. We introduce the rescaled variables defined by $z = L\bar{z}$, $t = L^2\bar{t}/D_s$ and $T = T_{\mathrm{mn}} + \mathcal{T}\bar{T}$, so that heat equation and initial condition become

$$\frac{\partial \bar{T}}{\partial \bar{t}} = \frac{\partial^2 \bar{T}}{\partial \bar{z}^2}\,, \tag{B.3}$$

$$\bar{T}\left(\bar{z}, 0\right) = 0\,. \tag{B.4}$$

The value of $\mathcal{T}$ will be determined by the boundary condition at the soil surface. Firstly, let us define the variable quantities Q_{net} and T_{a} in terms of the relative changes with respect to the average values rather than absolute changes, i.e., we write

$$\begin{aligned} Q_{\mathrm{net}}(t) &= Q_{\mathrm{av}}\left(1 + \bar{f}(t)\right)\,, \\ T_{\mathrm{a}}(t) &= T_{\mathrm{av}}\left(1 + \bar{g}(t)\right)\,. \end{aligned}$$

Using the same approach as for obtaining $f(t)$ and $g(t)$ in section 2, obtaining

$$\bar{f}(t) = \quad \frac{\pi}{2}\sin\left(\frac{2\pi t}{p_1}\right) - 1\,, \tag{B.5}$$

$$\bar{g}(t) = \quad \frac{T_{\mathrm{mn}}}{T_{\mathrm{av}}} - \frac{\Delta T}{2T_{\mathrm{av}}}\cos\left(\frac{2\pi\left(t - t_{\mathrm{min}}\right)}{p_2}\right) - 1\,, \tag{B.6}$$

The definition of G in (B.2) can be rearranged to be expressed in terms of a non-dimensional function $\bar{G}$

$$\begin{aligned} G(t) &= (1 - F_{VC})(1 - A_s)Q_{\mathrm{net}}(t) + H_{as}T_{\mathrm{a}}(t) \\ &= C_1 + (1 - F_{VC})(1 - A_s)Q_{\mathrm{av}}\bar{f}(t) + H_{as}T_{\mathrm{av}}\bar{g}(t) \\ &= C_1\left(1 + \beta_1\bar{f}(t) + (1 - \beta_1)\bar{g}(t)\right) \\ &= C_1\left(1 + \bar{G}\left(\bar{t}\right)\right)\,, \end{aligned} \tag{B.7}$$

where we have introduced the non-dimensional parameter

$$\beta_1 = \frac{(1 - F_{VC})(1 - A_s)Q_{\mathrm{av}}}{C_1}\,. \tag{B.8}$$

Upon using the non-dimensional quantities, the boundary condition at the surface becomes

$$-\left.\frac{k_s\mathcal{T}}{C_1 L}\frac{\partial \bar{T}}{\partial \bar{z}}\right|_{\bar{z}=0} = 1 + \bar{G}\left(\bar{t}\right) - \frac{C_2}{C_1}(T_{\mathrm{mn}} + \mathcal{T}\bar{T}(0, \bar{t}))\,. \tag{B.9}$$

Thus, if one takes $\mathcal{T} = LC_1/k_s$, then

$$-\left.\frac{\partial \bar{T}}{\partial \bar{z}}\right|_{\bar{z}=0} = \beta_2 + \bar{G}(\bar{t}) - \beta_3\bar{T}(0, \bar{t})\,. \tag{B.10}$$

where we have introduced the dimensionless parameters

$$\beta_2 = 1 - \frac{C_2 T_{\mathrm{mn}}}{C_1}\,, \qquad \beta_3 = \frac{C_2 \mathcal{T}}{C_1}\,, \tag{B.11}$$

As for the boundary condition at the end of the soil, it simply reads

$$\left.\frac{\partial \bar{T}}{\partial \bar{z}}\right|_{\bar{z}=1} = 0. \tag{B.12}$$

Appendix B.2. Eigenfunction Expansion

The problem to be solved is defined by the heat equation (B.3) subject to the boundary conditions (B.10) and (B.12) and the initial condition (B.4). Upon writing

$$u\left(x,\bar{t}\right) = \bar{T}\left(1-x,\bar{t}\right) - \frac{\beta_2 + \bar{G}\left(\bar{t}\right)}{\beta_3}\,, \tag{B.13}$$

one has the following system

$$\begin{aligned}
&\frac{\partial u}{\partial \bar{t}} + \frac{\bar{G}'}{\beta_3} = \frac{\partial^2 u}{\partial x^2}\,,\\
&\left.\frac{\partial u}{\partial x}\right|_{x=1} + \beta_3 u\left(1,\bar{t}\right) = \left.\frac{\partial u}{\partial x}\right|_{x=0} = 0\,,\\
&u\left(x,0\right) = -\frac{\beta_2 + \bar{G}(0)}{\beta_3}\,,
\end{aligned} \tag{B.14}$$

whose solution can be written in terms of the following generalised Fourier series:

$$u\left(x,\bar{t}\right) = \sum_{n=1}^{\infty} \varphi_n\left(\bar{t}\right)\cos\left(\lambda_n x\right)\,, \tag{B.15}$$

where λ_n are the positive solutions of

$$\tan\left(\lambda_n\right) = \frac{\beta_3}{\lambda_n}\,. \tag{B.16}$$

In what follows we shall use that 1 may be expressed as this same generalised Fourier series like:

$$1 = \sum_{n=1}^{\infty} b_n \cos(\lambda_n x)\,, \tag{B.17}$$

where

$$b_n = \frac{2\sin(\lambda_n)}{\lambda_n + \sin(\lambda_n)\cos(\lambda_n)} = \frac{2\beta_3\cos(\lambda_n)}{\lambda_n^2 + \beta_3\cos^2(\lambda_n)} \tag{B.18}$$

where we have used (B.16). Therefore, the initial condition is now

$$u(x,0) = -\frac{\beta_2 + \bar{G}(0)}{\beta_3} \sum_{n=1}^{\infty} b_n \cos(\lambda_n x)\,, \tag{B.19}$$

and so $\varphi_n(\bar{t})$ are the solutions of

$$\begin{aligned} \varphi_n' + \frac{\bar{G}'(\bar{t})}{\beta_3} b_n &= -\lambda_n^2 \varphi\,, \\ \varphi(0) &= -\frac{\beta_2 + \bar{G}(0)}{\beta_3} b_n\,. \end{aligned} \tag{B.20}$$

Therefore,

$$\begin{aligned} \varphi_n(\bar{t}) =& \frac{2\cos(\lambda_n)}{\lambda_n^2 + \beta_3 \cos^2(\lambda_n)} \left[\lambda_n^2 \int_0^{\bar{t}} \exp\left(-\lambda_n^2 \left(\bar{t} - \tau\right)\right) \bar{G}(\tau)\,\mathrm{d}\tau \right. \\ & \left. - \bar{G}(\bar{t}) - \beta_2 \exp\left(-\lambda_n^2 \bar{t}\right) \right]. \end{aligned} \tag{B.21}$$

Finally, due to the expression of $\bar{G}$, we can write the integral as

$$\begin{aligned} \int_0^{\bar{t}} \exp\left(-\lambda_n^2 \left(\bar{t} - \tau\right)\right) \bar{G}(\tau)\,\mathrm{d}\tau =& \beta_1 \int_0^{\bar{t}} \exp\left(-\lambda_n^2 \left(\bar{t} - \tau\right)\right) \bar{f}(\tau)\,\mathrm{d}\tau \\ & + (1-\beta_1) \int_0^{\bar{t}} \exp\left(-\lambda_n^2 \left(\bar{t} - \tau\right)\right) \bar{g}(\tau)\,\mathrm{d}\tau \\ =& \beta_1 \bar{I}_{1,n}(\bar{t}) + (1-\beta_1) \bar{I}_{2,n}(\bar{t})\,, \end{aligned} \tag{B.22}$$

where $\bar{I}_{1,n}$, $\bar{I}_{2,n}$ are easily obtained integrating by parts:

$$\begin{aligned} \bar{I}_{1,n}\left(\bar{t}\right) =& \frac{\bar{p}_1 \pi}{8\pi^2 + 2\bar{p}_1^2 \lambda_n^4} \left[\bar{p}_1 \lambda_n^2 \sin\left(\frac{2\pi \bar{t}}{\bar{p}_1}\right) - 2\pi \cos\left(\frac{2\pi \bar{t}}{\bar{p}_1}\right) \right. \\ & \left. + 2\pi \exp\left(-\lambda_n^2 \bar{t}\right) \right] - \frac{1}{\lambda_n^2} \left(1 - \exp\left(-\lambda_n^2 \bar{t}\right)\right)\,, \end{aligned} \tag{B.23}$$

$$\begin{aligned} \bar{I}_{2,n}\left(\bar{t}\right) =& \frac{1}{\lambda_n^2} \left(\frac{T_{\mathrm{mn}}}{T_{\mathrm{av}}} - 1\right) \left(1 - \exp\left(-\lambda_n^2 \bar{t}\right)\right) + \frac{\Delta T \bar{p}_2^2 \lambda_n^2}{2 T_{\mathrm{av}} \left(4\pi^2 + \bar{p}_2^2 \lambda_n^4\right)} \\ & \times \left[\exp\left(-\lambda_n^2 \bar{t}\right) \cos\left(\frac{2\pi \bar{t}_{\mathrm{min}}}{\bar{p}_2}\right) - \cos\left(\frac{2\pi \left(\bar{t} - \bar{t}_{\mathrm{min}}\right)}{\bar{p}_2}\right) \right] \\ & - \frac{\Delta T \bar{p}_2 \pi}{T_{\mathrm{av}} \left(4\pi^2 + \bar{p}_2^2 \lambda_n^4\right)} \left[\exp\left(-\lambda_n^2 \bar{t}\right) \sin\left(\frac{2\pi \bar{t}_{\mathrm{min}}}{\bar{p}_2}\right) \right. \\ & \left. + \sin\left(\frac{2\pi \left(\bar{t} - \bar{t}_{\mathrm{min}}\right)}{\bar{p}_2}\right) \right]. \end{aligned} \tag{B.24}$$

Then, the solution for the non-dimensional temperature in terms of $(\bar{z}, \bar{t})$ is given by

$$\begin{aligned}\bar{T}(\bar{z}, \bar{t}) = \sum_{n=1}^{\infty} \frac{2\cos(\lambda_n)\cos(\lambda_n(1-\bar{z}))}{\lambda_n^2 + \beta_3 \cos^2(\lambda_n)} \Big[& \beta_2 \left(1 - \exp\left(-\lambda_n^2 \bar{t}\right)\right) \\ & + \lambda_n^2 \left(\beta_1 \bar{I}_{1,n}(\bar{t}) + (1-\beta_1)\bar{I}_{2,n}(\bar{t})\right) \Big] ,\end{aligned} \tag{B.25}$$

with λ_n as the set of positive solutions of

$$\tan(\lambda_n) = \frac{\beta_3}{\lambda_n} . \tag{B.26}$$

Appendix B.2.1. Non perfect insulation

In this section we consider the case where the thermal insulation of the roof is not perfect and therefore some heat loss takes places at the lower boundary. We will write this as

$$-k_s \left. \frac{\partial T}{\partial z} \right|_{z=L} = C_1 \epsilon > 0 , \tag{B.27}$$

which relates the heat loss in the bottom of the soil to the heat gain occurring at its surface. In the non-dimensional formulation, this boundary condition corresponds to

$$-\left. \frac{\partial \bar{T}}{\partial \bar{z}} \right|_{\bar{z}=1} = \epsilon . \tag{B.28}$$

In this case we start by writing

$$v\left(x, \bar{t}\right) = \bar{T}\left(1 - x, \bar{t}\right) - \frac{\beta_2 + \bar{G}\left(\bar{t}\right)}{\beta_3} + \epsilon \left(\frac{\beta_3 + 1}{\beta_3} - x \right) , \tag{B.29}$$

which yields

$$\left. \frac{\partial v}{\partial x} \right|_{x=0} = -\left. \frac{\partial \bar{T}}{\partial \bar{z}} \right|_{\bar{z}=1} - \epsilon = 0 , \tag{B.30}$$

and

$$\begin{aligned}\left. \frac{\partial v}{\partial x} \right|_{x=1} &= -\left. \frac{\partial \bar{T}}{\partial \bar{z}} \right|_{\bar{z}=0} - \epsilon \\ &= \beta_2 + \bar{G}(\bar{t}) - \beta_3 \bar{T}(0, \bar{t}) - \epsilon \\ &= \beta_2 + \bar{G}(\bar{t}) - \beta_3 \left[v(1, \bar{t}) + \frac{\beta_2 + \bar{G}\left(\bar{t}\right)}{\beta_3} - \frac{\epsilon}{\beta_3} \right] - \epsilon \\ &= -\beta_3 v(1, \bar{t}) ,\end{aligned} \tag{B.31}$$

and therefore the original system can now be written as

$$
\begin{aligned}
&\frac{\partial v}{\partial \bar{t}} + \frac{\bar{G}'}{\beta_3} = \frac{\partial^2 v}{\partial x^2}\,, \\
&\left.\frac{\partial v}{\partial x}\right|_{x=1} + \beta_3 v\,(1,\bar{t}) = \left.\frac{\partial v}{\partial x}\right|_{x=0} = 0\,, \\
&v\,(x,0) = -\frac{\beta_2 + \bar{G}(0)}{\beta_3} + \epsilon\left(\frac{\beta_3+1}{\beta_3} - x\right)\,.
\end{aligned}
\tag{B.32}
$$

Similarly as before, we obtain

$$
v\,(x,\bar{t}) = \sum_{n=1}^{\infty} \phi_n\,(\bar{t})\cos\left(\lambda_n x\right)\,, \tag{B.33}
$$

where λ_n are again the positive solutions of equation (B.16).

The procedure is now the same as before except for the fact that now

$$
v(x,0) = -\frac{\beta_2 + \bar{G}(0)}{\beta_3}\sum_{n=1}^{\infty} b_n \cos(\lambda_n x) + \epsilon \sum_{n=1}^{\infty} c_n \cos(\lambda_n x)\,, \tag{B.34}
$$

where b_n is provided in (B.18) and

$$
c_n = \frac{2}{\lambda_n^2 + \beta_3\cos^2(\lambda_n)}\,. \tag{B.35}
$$

Therefore, $\phi_n(\bar{t})$ are the solutions of

$$
\begin{aligned}
&\phi_n' + \frac{\bar{G}'(\bar{t})}{\beta_3} b_n = -\lambda_n^2 \phi_n\,, \\
&\phi_n(0) = -\frac{\beta_2 + \bar{G}(0)}{\beta_3} b_n + \epsilon c_n\,.
\end{aligned}
\tag{B.36}
$$

Therefore,

$$
\begin{aligned}
\phi_n(\bar{t}) &= \phi_n(0)\exp(-\lambda^2\bar{t}) - \frac{b_n}{\beta_3}\int_0^{\bar{t}} \exp\left(-\lambda^2(\bar{t}-\tau)\right)\bar{G}'(\tau)\mathrm{d}\tau \\
&= -\left(\frac{\beta_2}{\beta_3} b_n - \epsilon c_n\right)\exp(-\lambda^2\bar{t}) - \frac{b_n}{\beta_3}\Bigg[\bar{G}(\bar{t}) \\
&\quad + \lambda_n^2 \int_0^{\bar{t}} \exp\left(-\lambda^2(\bar{t}-\tau)\right)\bar{G}(\tau)\mathrm{d}\tau\Bigg]\,.
\end{aligned}
\tag{B.37}
$$

Then, the solution for the non-dimensional temperature in terms of $(\bar{z}, \bar{t})$ when the roof transfers energy to the house is given by

$$
\begin{aligned}
\bar{T}(\bar{z}, \bar{t}) =& \sum_{n=1}^{\infty} \frac{b_n}{\beta_3} \Bigg[\left(\beta_2 - \epsilon \frac{\beta_3 c_n}{b_n} \right) \left(1 - \exp(-\lambda_n^2 \bar{t}) \right) \\
& + \lambda_n^2 \left(\beta_1 \bar{I}_{1,n}(\bar{t}) + (1-\beta_1) \bar{I}_{2,n}(\bar{t}) \right) \Bigg] \cos\left(\lambda_n (1-\bar{z})\right) \\
=& \sum_{n=1}^{\infty} \frac{b_n}{\beta_3} \Bigg[\left(\beta_2 - \frac{\epsilon}{\cos(\lambda_n)} \right) \left(1 - \exp(-\lambda_n^2 \bar{t}) \right) \\
& + \lambda_n^2 \left(\beta_1 \bar{I}_{1,n}(\bar{t}) + (1-\beta_1) \bar{I}_{2,n}(\bar{t}) \right) \Bigg] \cos\left(\lambda_n (1-\bar{z})\right) ,
\end{aligned}
\tag{B.38}
$$

with λ_n is given in (B.26) and $I_{1,n}$, $I_{2,n}$ are provided in (B.23) and (B.24). From equation (B.26) we also find $\cos(\lambda_n) \sim (-1)^n$ for large values of n. In particular, note how the solution (B.38) reduces to (B.25) when we set $\epsilon = 0$.

Appendix B.3. Total energy absorbed

To compute the expression for the energy absorbed we shall use expressions (23):

$$
\begin{aligned}
E(t) =& \int_0^L \rho_s c_s \left(T(z,t) - T_{\mathrm{mn}} \right) \mathrm{d}z = \frac{L^2 C_1 \rho_s c_s}{k_s} \int_0^1 \bar{T}\left(\bar{z}, \frac{L^2 t}{D_s} \right) \mathrm{d}\bar{z} \\
=& \frac{L^2 C_1 \rho_s c_s}{k_s} \sum_{n=1}^{\infty} \left\{ \frac{2\cos(\lambda_n)\sin(\lambda_n)}{\lambda_n^3 + \beta_3 \lambda_n \cos^2(\lambda_n)} \left[\beta_2 \left(1 - \exp\left(-\lambda_n^2 \frac{L^2 t}{D_s} \right) \right) \right. \right. \\
& \left. \left. + \lambda_n^2 \left(\beta_1 I_{1,n}(t) + (1-\beta_1) I_{2,n}(t) \right) \right] \right\} ,
\end{aligned}
$$

where $I_{i,n}(t) = \bar{I}_{i,n}\left(L^2 t / D_s \right)$. We note that

$$
\frac{\cos(\lambda_n)\sin(\lambda_n)}{\lambda_n^3 + \beta_3 \lambda_n \cos^2(\lambda_n)} = \frac{\beta_3}{\lambda_n^4 + \lambda_n^2 \beta_3 (1+\beta_3)} , \tag{B.39}
$$

where we recall that $\beta_3 = C_2 L / k_s$. To compute the energy absorbed at the end of the day we must simply evaluate this expression at t_f. We note that the above expression converges very fast. Indeed, one can even use the expression obtained by just retaining the first term:

$$
\begin{aligned}
E(t_f) \sim& \frac{2 L^2 C_1 \rho_s c_s \beta_3}{k_s \left(\lambda_1^4 + \lambda_1^2 \beta_3 (1+\beta_3) \right)} \left[\beta_2 \left(1 - \exp\left(-\lambda_n^2 \frac{L^2 t}{D_s} \right) \right) \right. \\
& \left. + \lambda_1^2 \left(\beta_1 I_{1,1}\left(\frac{L^2 t_f}{D_s} \right) + (1-\beta_1) I_{2,1}\left(\frac{L^2 t_f}{D_s} \right) \right) \right] ,
\end{aligned}
\tag{B.40}
$$

where $\lambda_1 \in \left(0, \frac{\pi}{2}\right)$ is the unique solution of (B.26) for $n = 1$.

Appendix B.3.1. Non perfect insulation

In the case where heat is transferred to the building, we combine (23) and (B.38) and obtain

$$E(t) = \frac{L^2 C_1 \rho_s c_s}{k_s} \sum_{n=1}^{\infty} \frac{2\beta_3}{\lambda_n^4 + \lambda_n^2 \beta_3 (1+\beta_3)} \left[\left(\beta_2 - \frac{\epsilon}{\cos(\lambda_n)}\right) \left(1 - \exp\left(-\lambda_n^2 \frac{L^2 t}{D_s}\right)\right) \right.$$
$$\left. + \lambda_n^2 \left(\beta_1 I_{1,n}\left(\frac{L^2 t}{D_s}\right) + (1-\beta_1)\, I_{2,n}\left(\frac{L^2 t}{D_s}\right)\right) \right].$$

Therefore, the corresponding approximate expression for the total energy stored at the end of the day reads:

$$E(t_f) \sim \frac{L^2 C_1 \rho_s c_s}{k_s} \frac{2\beta_3}{\lambda_1^4 + \lambda_1^2 \beta_3 (1+\beta_3)} \left[\left(\beta_2 - \frac{\epsilon}{\cos(\lambda_1)}\right) \left(1 - \exp\left(-\lambda_1^2 \frac{L^2 t}{D_s}\right)\right) \right.$$
$$\left. + \lambda_1^2 \left(\beta_1 I_{1,1}\left(\frac{L^2 t_f}{D_s}\right) + (1-\beta_1)\, I_{2,1}\left(\frac{L^2 t_f}{D_s}\right)\right) \right].$$

Appendix B.4. Approximate expression for λ_1

We now focus on (B.26) and we shall derive an approximate explicit expression for the first eigenvalue, λ_1. Since the first eigenvalue has a value lower than $\pi/2$, we define $z = 2/\pi\lambda_1$ and so z is expected to be small. Therefore, Taylor expanding the tangent one reaches

$$\frac{\pi}{2} z \left(\frac{\pi}{2} z + \frac{\pi^3}{24} z^3 + \frac{\pi^5}{240} z^5 + \mathcal{O}(z^7) \right) = \beta_3 \,, \tag{B.41}$$

whose only positive real solution is

$$\lambda_1 \approx \left(\frac{5^{1/3}}{6} y - \frac{5}{6} - \frac{13 \cdot 5^{2/3}}{6y} \right)^{1/2} , \tag{B.42}$$

where

$$y = \left(110 + 162\beta_3 + 9\sqrt{285 + 440\beta_3 + 324\beta_3^2} \right)^{1/3} . \tag{B.43}$$

References

[1] M. Antrop, Landscape change and the urbanization process in Europe, Landscape and Urban Planning 67 (1-4) (2004) 9–26. doi:10.1016/S0169-2046(03)00026-4.

[2] H. Ritchie, M. Roser, Urbanization, Our World in Data (2018). URL `https://ourworldindata.org/urbanization`

[3] L. Howard, The Climate of London: Deduced from Meteorological Observations made in the Metropolis and at Various Places around it, Harvey and Darton, J. and A. Arch, Longman, Hatchard, S. Highley and R. Hunter, 1833.

[4] H. Landsberg, The Urban Climate, Academic Press, 1981.

[5] A. Mohajerani, J. Bakaric, T. Jeffrey-Bailey, The urban heat island effect, its causes, and mitigation, with reference to the thermal properties of asphalt concrete, Journal of Environmental Management 197 (2017) 522–538. `doi:10.1016/j.jenvman.2017.03.095`.

[6] K. Deilami, M. Kamruzzaman, Y. Liu, Urban heat island effect: A systematic review of spatio-temporal factors, data, methods, and mitigation measures, International Journal of Applied Earth Observation and Geoinformation 67 (2018) 30–42. `doi:10.1016/j.jag.2017.12.009`.

[7] M. Baccini, A. Biggeri, G. Accetta, T. Kosatsky, K. Katsouyanni, A. Analitis, H. R. Anderson, L. Bisanti, D. D'Ippoliti, J. Danova, B. Forsberg, S. Medina, A. Paldy, D. Rabczenko, C. Schindler, P. Michelozzi, Heat effects on mortality in 15 European cities, Epidemiology (2008) 711–719`doi:10.1097/EDE.0b013e318176bfcd`.

[8] R. Basu, High ambient temperature and mortality: a review of epidemiologic studies from 2001 to 2008, Environmental Health 8 (1) (2009) 1–13.

[9] C. Heaviside, H. Macintyre, S. Vardoulakis, The urban heat island: implications for health in a changing environment, Current Environmental Health Reports 4 (3) (2017) 296–305.

[10] J.-M. Robine, S. L. K. Cheung, S. Le Roy, H. Van Oyen, C. Griffiths, J.-P. Michel, F. R. Herrmann, Death toll exceeded 70,000 in Europe during the summer of 2003, Comptes Rendus Biologies 331 (2) (2008) 171–178, dossier : Nouveautés en cancérogenèse / New developments in carcinogenesis. `doi:10.1016/j.crvi.2007.12.001`.

[11] Environmental Protection Agency US, Heat islands, `https://www.epa.gov/heatislands/heat-island-cooling-strategies` (2021).

[12] P. Bevilacqua, D. Mazzeo, R. Bruno, N. Arcuri, Surface temperature analysis of an extensive green roof for the mitigation of urban heat island in southern mediterranean climate, Energy and Buildings 150 (2017) 318–327. doi:10.1016/j.enbuild.2017.05.081.

[13] A. Solcerova, F. van de Ven, M. Wang, M. Rijsdijk, N. van de Giesen, Do green roofs cool the air?, Building and Environment 111 (2017) 249–255. doi:10.1016/j.buildenv.2016.10.021.

[14] J. Yang, D. llamathy Mohan Kumar, A. Pyrgou, A. Chong, M. Santamouris, D. Kolokotsa, S. E. Lee, Green and cool roofs' urban heat island mitigation potential in tropical climate, Solar Energy 173 (2018) 597–609. doi:10.1016/j.solener.2018.08.006.

[15] J. Berndtsson, Green roof performance towards management of runoff water quantity and quality: A review, Ecological Engineering 36 (4) (2010) 351–360. doi:10.1016/j.ecoleng.2009.12.014.

[16] S.-X. Li, H.-P. Qin, Y.-N. Peng, S. T. Khu, Modelling the combined effects of runoff reduction and increase in evapotranspiration for green roofs with a storage layer, Ecological Engineering 127 (2019) 302–311. doi:10.1016/j.ecoleng.2018.12.003.

[17] W. Liu, B. A. Engel, Q. Feng, Modelling the hydrological responses of green roofs under different substrate designs and rainfall characteristics using a simple water balance model, Journal of Hydrology 602 (2021) 126786. doi:10.1016/j.jhydrol.2021.126786.

[18] L. Locatelli, O. Mark, P. S. Mikkelsen, K. Arnbjerg-Nielsen, M. Bergen Jensen, P. J. Binning, Modelling of green roof hydrological performance for urban drainage applications, Journal of Hydrology 519 (2014) 3237–3248. doi:10.1016/j.jhydrol.2014.10.030.

[19] K. Abhijith, P. Kumar, J. Gallagher, A. McNabola, R. Baldauf, F. Pilla, B. Broderick, S. Di Sabatino, B. Pulvirenti, Air pollution abatement performances of green infrastructure in open road and built-up street canyon environments – a review, Atmospheric Environment 162 (2017) 71–86. doi:10.1016/j.atmosenv.2017.05.014.

[20] Q. Zhang, L. Miao, X. Wang, D. Liu, L. Zhu, B. Zhou, J. Sun, J. Liu, The capacity of greening roof to reduce stormwater runoff and pollution, Landscape and Urban Planning 144 (2015) 142–150. doi:10.1016/j.landurbplan.2015.08.017.

[21] S. Quezada-Garcia, G. Espinosa-Paredes, M. A. Polo-Labarrios, E. G. Espinosa-Martinez, M. A. Escobedo-Izquierdo, Green roof heat and mass transfer mathematical models: A review, Building and Environment 170 (2020) 106634. doi:10.1016/j.buildenv.2019.106634.

[22] D. Sailor, A green roof model for building energy simulation programs, Energy and Buildings 40 (8) (2008) 1466 – 1478. doi:10.1016/j.enbuild.2008.02.001.

[23] L. Cirrincione, G. Peri, Covering the gap for an effective energy and environmental design of green roofs: Contributions from experimental and modelling researches, in: Rethinking Sustainability Towards a Regenerative Economy. Future City, Springer, Cham, 2021. doi:10.1007/978-3-030-71819-0_8.

[24] T. Myers, N. Fowkes, A. Fareo, S. Goqo, Estimating the effect of green roofs on a city's energy footprint, in: Proceedings of the Mathematics in Industry Study Group 2020, University of the Witwatersrand, 2020, pp. 1–21, 2020 Mathematics in Industry Study Group, MISG 2020 ; Conference date: 28-01-2020 Through 01-02-2020.

[25] J. R. Philip, D. A. De Vries, Moisture movement in porous materials under temperature gradients, Eos, Transactions American Geophysical Union 38 (2) (1957) 222–232. doi:10.1029/TR038i002p00222.

[26] E. Palomo del Barrio, Analysis of the green roofs cooling potential in buildings, Energy and Buildings 27 (2) (1998) 179 – 193. doi:10.1016/S0378-7788(97)00029-7.

[27] J. Kondo, N. Saigusa, Modelling the evaporation from bare soil with a formula for vaporization in the soil pores, Journal of the Meteorological Society of Japan. Ser. II 72 (3) (1994) 413–421. doi:10.2151/jmsj1965.72.3_413.

[28] D. Sailor, A green roof model for building energy simulation programs, Energy and Buildings 40 (8) (2008) 1466–1478. doi:10.1016/j.enbuild.2008.02.001.

[29] S. E. Ouldboukhitine, R. Belarbi, I. Jaffal, A. Trabelsi, Assessment of green roof thermal behavior: A coupled heat and mass transfer model, Building and Environment 46 (12) (2011) 2624–2631. doi:10.1016/j.buildenv.2011.06.021.

[30] C. J. van der Kooi, P. G. Kevan, M. H. Koski, The thermal ecology of flowers, Annals of Botany XX (2019) 1–11. doi:10.1093/aob/mcz073.

[31] B. R. Helliker, S. L. Richter, Subtropical to boreal convergence of tree-leaf temperatures, Nature 454 (2008) 511–514. doi:10.1038/nature07031.

[32] E. T. Linacre, Further notes on a feature of leaf and air temperatures, Archiv für Meteorologie, Geophysik und Bioklimatologie B15 (1967) 422–436. doi:10.1007/BF02390453.

[33] S. T. Michaletz, M. D. Weiser, J. Zhou, M. Kaspari, B. R. Helliker, B. J. Enquist, Plant thermoregulation: Energetics, trait–environment interactions, and carbon economics, Trends in Ecology and Evolution 30 (12) (2015) 714–724. doi:10.1016/j.tree.2015.09.006.

[34] A. Ávila-Hernández, E. Simá, J. Xamán, I. Hernández-Pérez, E. Téllez-Velázquez, M. A. Chagolla-Aranda, Test box experiment and simulations of a green-roof: Thermal and energy performance of a residential building standard for Mexico, Energy and Buildings 209 (2020) 109709. doi:https://doi.org/10.1016/j.enbuild.2019.109709.

[35] D. J. Watson, Comparative Physiological Studies on the Growth of Field Crops: I. Variation in Net Assimilation Rate and Leaf Area between Species and Varieties, and within and between Years, Annals of Botany 11 (1) (1947) 41–76. doi:10.1093/oxfordjournals.aob.a083148.

[36] J. Coma, A. de Gracia, M. Chàfer, G. Pérez, L. F. Cabeza, Thermal characterization of different substrates under dried conditions for extensive green roofs, Energy and Buildings 144 (2017) 175–180. doi:10.1016/j.enbuild.2017.03.031.

[37] P. Bevilacqua, D. Mazzeo, R. Bruno, N. Arcuri, Experimental investigation of the thermal performances of an extensive green roof in the mediterranean area, Energy and Buildings 122 (2016) 63–79. doi:10.1016/j.enbuild.2016.03.062.

[38] R. C. Dorf (Ed.), The Engineering Handbook, CRC Press, USA, 2004.

[39] A. El Mir, A. Pèity, S. G. Nehme, Effect of maximum aggregate size on mechanical properties of high-strength concrete, in: Proc. 12th Central European Congress on Concrete Engineering, 2017, pp. 233–239.

[40] V. Kodur, W. Khaliq, Effect of temperature on thermal properties of different types of high-strength concrete, Journal of Materials in Civil Engineering 23 (6) (2011) 793–801. doi:10.1061/(ASCE)MT.1943-5533.0000225.

[41] J. Hill, J. Drake, B. Sleep, Comparisons of extensive green roof media in Southern Ontario, Ecological Engineering 94 (2016) 418–426. doi:10.1016/j.ecoleng.2016.05.045.

[42] M. R. Granados, S. Bonachela, J. Hernández, J. C. López, J. J. Pérez-Parra, E. J. Baeza, J. J. Magán, Measurement of the soil-air convective heat transfer coefficient from a greenhouse mulch soil, Acta Horticulturae 893 (2011) 539–544. doi:10.17660/ActaHortic.2011.893.55.

[43] S. J. Allen, J. S. Wallace, J. H. C. Gash, M. V. K. Sivakumar, Measurements of albedo variation over natural vegetation in the sahel, International Journal of Climatology 14 (6) (1994) 625–636. doi:10.1002/joc.3370140603.

[44] M. Pomerantz, H. Akbari, S.-C. Chang, R. M. Levinson, B. Pon, Examples of cooler reflective streets for urban heat-island mitigation : Portland cement concrete and chip seals, Tech. rep., Lawrence Berkeley National Laboratory, added to JabRef: 2010.04.28 (04 2003).
URL http://repositories.cdlib.org/lbnl/LBNL-49283

[45] H. Li, J. Harvey, A. Kendall, Field measurement of albedo for different land cover materials and effects on thermal performance,, Building and Environment 59 (2017) 536–546. doi:10.1016/j.buildenv.2012.10.014.

[46] M. Hulley, The urban heat island effect: causes and potential solutions, in: F. Zeman (Ed.), Metropolitan Sustainability, Woodhead Publishing, 2012, pp. 79–98. doi:10.1533/9780857096463.1.79.

[47] N. An, S. Hemmati, Y.-J. Cui, Assessment of the methods for determining net radiation at different time-scales of meteorological variables, Journal of Rock Mechanics and Geotechnical Engineering 9 (2) (2017) 239–246. doi:10.1016/j.jrmge.2016.10.004.

[48] Y. Qin, J. Liang, Z. Huang, K. Tan, Painting the roadway embankment with non-white high reflective pigments to raise the albedo, Environmental Earth Sciences 75 (4) (2016) 359. doi:10.1007/s12665-016-5273-6.

[49] C. YU, The intervention of plants in the conflicts between buildings and climate - a case study in singapore (2006).

[50] C. L. Tan, N. H. Wong, P. Y. Tan, S. K. Jusuf, Z. Q. Chiam, Impact of plant evapotranspiration rate and shrub albedo on temperature reduction in the tropical outdoor environment, Building and Environment 94 (2015) 206–217. doi:https://doi.org/10.1016/j.buildenv.2015.08.001.
URL https://www.sciencedirect.com/science/article/pii/S0360132315300822

[51] A. Khalifa, R. Marshall, Validation of heat transfer coefficients on interior building surfaces using a real-sized indoor test cell, International Journal of Heat and Mass Transfer 33 (10) (1990) 2219–2236. doi:https://doi.org/10.1016/0017-9310(90)90122-B.
URL https://www.sciencedirect.com/science/article/pii/001793109090122B

[52] T. Cholewa, R. Anasiewicz, A. Siuta-Olcha, M. A. Skwarczynski, On the heat transfer coefficients between heated/cooled radiant ceiling and room, Applied Thermal Engineering 117 (2017) 76–84. doi:https://doi.org/10.1016/j.applthermaleng.2017.02.019.
URL https://www.sciencedirect.com/science/article/pii/S1359431117307834